

# Gamma-Ray Bursts

Version: June 2, 2022

*Edited by*

C. Kouveliotou, S.E. Woosley, L. Piro



## 6

# Discoveries enabled by Multi-wavelength Afterglow Observations of Gamma-Ray Bursts

Jochen Greiner, MPE, Giessenbachstr. 1, 85740 Garching, Germany

### 6.1 Introduction

The progress in the Gamma-Ray Burst (GRB) field over the last decade and prior to the launch of *Fermi* mostly occurred in our understanding of the afterglow emission and the GRB surroundings. Classical observational astronomy, from the radio to X-rays, played a vital role in this progress as it allowed the identification of GRB counterparts by drastically improving the position accuracy of the bursters down to the sub-arcsec level. Once the afterglows were identified, the full power of optical and near-infrared instrumentation came to play, and resulted in an overwhelming diversity of observational results and consequently in the understanding of the properties of the relativistic outflows, their interaction with the circumsource medium, as well as the surrounding interstellar medium (ISM) and the host galaxies. Here we describe the basic multi-wavelength observational properties of afterglows, of both long- and short-duration GRBs, as obtained with space- (Tab. 6.1) and ground-based instruments. The present sample consists of  $\sim 550$  X-ray and  $\sim 350$  optical afterglows (see <http://www.mpe.mpg.de/~jcg/grbgen.html>).

Table 6.1. *Main Satellite-Missions contributing to the afterglow sample*

Mission/Years	Instrument	Energy range	Localisation	GRBs
BSAX: 1996–2002	GRBM	2–28 keV	omni-directional	
	WFC	2–28 keV	some arcmin	$\sim 30$ /yr
HETE-2: 2000–2006	FREGATE	6–400 keV	omni-directional	
	WXM	2–25 keV	10 arcmin	$\sim 10$ /yr
INTEGRAL 2001–	ACS	$>80$ keV	omni-directional	
	ISGRI	20–150 keV	3 arcmin	$\sim 10$ /yr
Swift: 2004–	BAT	15–150 keV	3 arcmin	$\sim 100$ /yr
AGILE: 2007–	SuperAGILE	10–40 keV	5 arcmin	$\sim 6$ /yr
Fermi: 2008–	GBM	8–30000 keV	some deg	$\sim 250$ /yr
	LAT	0.1–300 GeV	some arcmin	$\sim 7$ /yr

## 6.2 Early searches for transient optical emission

Over the first two decades after the discovery of GRBs (until 1996), GRB localizations were either *delayed but accurate*, e.g., with arcmin accuracy, as provided by the Interplanetary Network (*IPN* (Hurley et al., 1999) with typical delays of days or *rapid but rough*, e.g., within minutes after the GRB trigger, but with at least  $2^\circ$  error circles as provided by the BATSE Coordinate Distribution Network system (Barthelmy et al., 1996).

Correspondingly, several alternative strategies were pursued: (1) searching for quiescent emission in well-localized error boxes (assuming the existence of quiescent persistent GRB sources), (2) *post facto* correlating optical monitoring observations temporally overlapping with GRB triggers, and (3) quick follow-up observations after a GRB trigger.

### 6.2.1 Searching for persistent quiescent GRB emission

Archival searches for *optical* transients in small GRB error boxes using large photographic plate collections were initiated at Harvard Observatory (Schaefer et al., 1984), and then performed at several other observatories (Hudec et al., 1987; Greiner et al., 1987). Though more than 130 thousand plates were investigated (see Tab. 6.2) and several optical transients were found, no convincing GRB counterpart was identified except the 2008 report on GRB 920925C (Denisenko & Terekhov, 2008).

The first search for *quiescent X-ray* sources in 5 GRB error boxes was conducted with the *Einstein* (Pizzichini et al., 1986) and *EXOSAT* satellites (Boër et al., 1988). Greiner et al. (1995) extended these searches to the *ROSAT* all-sky-survey data for more than 30 (15) GRB error boxes determined with the 2<sup>nd</sup> (3<sup>rd</sup>) *IPN* catalogs. While a number of X-ray sources were found, their identification did not reveal any unusual associations, thus none of these X-ray sources was considered a quiescent GRB counterpart.

Table 6.2. *Archival Search for GRB optical counterparts*

Group	Observatories	No. of GRB error boxes	No. of plates	monitoring time (yrs)
Schaefer et al.	Harvard	16	32000	4.25
Hudec et al.	Ondřejov	21	30000	10
Greiner et al.	Sonneberg	15	35000	2.6
Moskalenko et al.	Odessa	40	40000	1.3
Schwartz et al.	S. Barbara	7	photoelectric	0.1

### 6.2.2 Post-facto correlation analysis

Historically, the hunt for GRB counterparts began with the systematic search in photographic exposures serendipitously taken during the burst event (Grindlay, Wright & McCrosky, 1974). This correlation approach was later extended substantially, and was also done in a variety of passbands, including scanning observations with the Cosmic Background Explorer (*COBE*) (Bontekoe et al., 1995).

In the optical band, regular, wide-field sky patrols of two kinds were correlated with GRBs detected with the *Compton Gamma-Ray Observatory (CGRO)/ Burst And Transient Source Experiment (BATSE)*: (i) the Explosive Transient Camera (ETC) exposures with a total field of view (FoV) of  $40^\circ \times 60^\circ$  (Vanderspek, Krimm & Ricker, 1995), and (ii) the logistic network of photographic patrols performed at a dozen observatories worldwide (Greiner et al., 1994). During over 4 years of operation there were five cases when a BATSE GRB occurred during an ETC observation within or near an ETC FoV. No optical transients were detected, resulting in upper limits for the fluence ratio of gamma to optical luminosities,  $L_\gamma/L_{opt} \geq 2\text{--}120$ . Unfortunately, in all cases of simultaneous exposures only a part (20%–80%) of the rather large BATSE error box ( $> 2^\circ$ ; see also Chapter 3) was covered. The correlation of BATSE GRBs with photographic wide-field plates of a network of 11 observatories identified simultaneous plates for nearly 60 GRBs, with typical limiting magnitudes of  $m_{lim} \approx 2\text{--}3$  mag for an 1 s duration flash (Greiner et al., 1994). These limits would correspond to a  $m_{lim} \approx 11\text{--}12$  mag for the canonical afterglow durations discovered in the *Swift* era (see also Chapter 5). Blink comparison of these plates did not reveal any optical transient (but it did find several new variable stars) resulting in limits for the flux ratio of gamma-rays to optical emission of  $F_\gamma/F_{opt} \geq 1\text{--}20$ . We know today that these limits were too high for the detection of a canonical optical afterglow. Instead, the non-detection of an optical counterpart for nearly 60 GRBs is consistent with very bright afterglows like e.g., GRB 990123 and 080319B being very rare, of order 1-2% of the total afterglow population.

### 6.2.3 Rapid follow-up observations of GRBs

Early rapid follow-up observations were done already well before the discovery of afterglows in 1997 (see also Chapter 4), but due to the relatively large GRB error boxes these searches were not successful in identifying a plausible counterpart. Already in the early 90s, these rapid follow-up observations relied on the BATSE COordinate DIstribution NETwork (BACODINE), which computed and distributed coordinates of bright GRBs (which had smaller

error boxes) within typically 5 sec after the GRB trigger to interested observers (Barthelmy et al., 1996). However, for the few bursts within the FoV of the imaging *CGRO*/COMPTON TELESCOPE (COMPTEL) coordinates were determined with much better accuracy and were distributed after typically 15–30 minutes after detection via the BATSE/COMPTEL/NMSU network (Kippen et al., 1994).

Both, optical and X-ray follow-up observations were performed in the 90's. Notably, GRB 940301 was observed seven hours after the GRB trigger with the 1 m Schmidt telescope at Socorro reaching a limiting magnitude of  $m_V \approx 16$  mag (Harrison et al., 1995); no optical transient was detected.

*ROSAT* pointed observations were initiated within 4 weeks of two GRBs, namely GRB 920501 (Li et al., 1996) and 940301, which due to their close locations had been dubbed “*COMPTEL* repeater” GRB 930704/ 940301 (Greiner et al., 1996). None revealed a fading X-ray counterpart.

### 6.3 The *BeppoSAX* afterglow discovery

The launch in 1996 of the Italian-Dutch Satellite per Astronomia X, *SAX*, ushered a major breakthrough in our understanding of GRBs (for a detailed description of the *SAX* results see also Chapter 4). Its unprecedented localization accuracy ( $\sim 5'$ ; 2–35 keV), rapid notification (within minutes of the GRB) was coupled with its fast slewing capability (a few hours) and re-pointing with its co-aligned narrow field X-ray telescopes. Despite the fact that only  $\approx 3.5\%$  of its total observing time (or 1.5% of all observations) was spent on GRBs, *BeppoSAX* brought a revolution in the field of GRBs allowing the tools of optical/NIR/radio astronomy to be applied to these fascinating objects.

The follow-up observation of GRB 970228 led to the discovery of the first X-ray and optical afterglow (Fig. 6.1) (Costa et al., 1997; Van Paradijs et al., 1997). The next important event, the rapid localization of GRB 970508, allowed the first measurement of the GRB distance scale via optical spectroscopy. GRB 970508 was also the burst with the first radio afterglow. These multi-wavelength observations provided the first observational evidence for the fireball scenario (Metzger et al., 1997; Frail et al., 1997). Subsequent measurements within the next two years demonstrated the extragalactic nature of GRBs through more redshift measurements of the optical afterglow emission as well as of the host galaxies, and firmly established GRBs as the most luminous objects known in the Universe. The year 1998 also saw the discovery of GRB 980425, which was subsequently associated with a supernova (SN 1998bw) (Galama et al., 1998a).

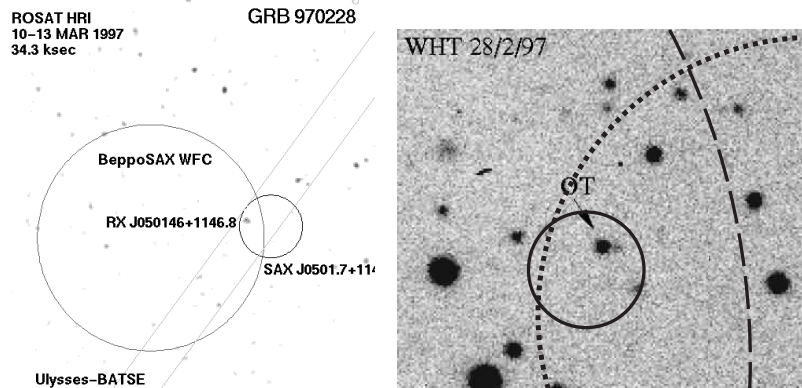


Fig. 6.1. Sequence of error circles from  $\gamma$ -rays to optical for GRB 970228, the first GRB for which long-wavelength afterglow emission was identified. Left: The underlying image is from a 34 ksec *ROSAT*/High-Resolution Imager (HRI) observation (Frontera et al., 1998), with the large circle showing the  $3\sigma$  error circle of the X-ray afterglow as determined with the *BeppoSAX*/Wide-Field Camera (WFC). The smaller circle is the  $\approx 1$  arcmin error circle of the fading source SAX J0501.7 + 1146 found with the two *BeppoSAX*/Narrow-Field instrument (NFI) pointings, and the two straight lines mark the triangulation circle derived from the *BeppoSAX* and *Ulysses* timings (Hurley et al., 1997). Right: Optical image taken on 1997 February 28 (Van Paradijs et al., 1997) at the William Herschel Telescope (Canary Islands) with the WFC error circle marked as a dashed segment, the NFI error circle with the dotted segment, and the  $10''$  *ROSAT*/HRI error box as a full circle. The optical transient (OT) falls right into the *ROSAT*/HRI error box.

During its lifetime, *BeppoSAX* observed 56 GRBs and slewed to 36 of these (Piro & Scarsi, 2004) within typically 5–24 hrs (average around 8 hrs). X-ray afterglows were discovered in over 90% of the cases and their fundamental properties were established. It was found that the X-ray flux fades with a power law dependence  $t^{-\alpha}$ , with  $\alpha \sim 1.4$  (Piro, 2001). The X-ray spectrum is well described with a power law  $\nu^{-\beta}$  of slope  $\beta \sim 0.9$ . The observed absorption is, within the errors, always compatible with the Galactic foreground absorption. The observed flux at a given time after the burst, which is proportional to  $(1+z)^{\beta-\alpha}$ , shows a pretty narrow distribution, since the cosmological spectral redshift (K correction) and temporal decay roughly compensate each other: the mean flux in the 1 – 10 keV band at 11 hrs after the burst is about  $5 \times 10^{-13}$  erg cm $^{-2}$  s $^{-1}$  (Piro, 2001). The overall energy emitted in this late afterglow phase ( $> 6 - 8$  hrs) is typically a few percent of the GRB energy.

We shortly note here two major results because *BeppoSAX* laid the foun-

dations for their studies: (i) Jet breaks: Being a geometrical effect, jet breaks in afterglow light curves are achromatic, and indeed a number of cases with such breaks at 0.5 – 1 days after the burst were detected. This provided the early observational evidence of beaming in GRBs. (ii) Confirmation of the basic synchrotron scenario: The broad-band spectral energy distribution (SED) was predicted to consist of four segments with different powerlaw slopes. The breaks in the SED were found only in very few cases, first in GRB 970508 (Wijers & Galama, 1999), but provided the first observational evidence of a rather low circumburst density ( $0.03 \text{ cm}^{-3}$ ) and a large equivalent isotropic energy ( $3 \times 10^{52}$  erg). Further details on both topics are given in Chapters 8 and 11.

#### 6.4 Multiwavelength observations

The detection of the first optical afterglow(s) sparked an international observing effort, which was unique, except perhaps for SN 1987A. All major ground-based telescopes were used at optical, infrared as well as in radio wavelengths, and basically every space-born observatory since then has observed GRBs. The *HETE-2* satellite (Ricker et al., 2002), launched in October 2000, continued to provide rapid and arcmin sized GRB localizations at a rate of about 2 per month after *BeppoSAX* had been switched off in April 2003. *Swift*, launched in November 2004, revolutionized our knowledge on the afterglow phenomena. Over the last 13 years (February 1997 – June 2010) a total of 870 GRBs have been localized within a day to less than one square-degree size error boxes, and X-ray afterglows have been detected basically for each of those bursts for which X-ray observations have been done within a few days (see <http://www.mpe.mpg.de/~jcg/grbgen.html>).

##### 6.4.1 Contemporaneous, prompt multiwavelength emission

Some optical afterglows have shown substantial variability at early times. One can distinguish a component which tracks the prompt gamma-rays (GRB 041219A (Vestrand et al., 2005; Blake et al., 2005), GRB 050820A (Vestrand et al., 2006), GRB 080319B (Racusin et al., 2008)) and an afterglow component which starts during or shortly after the prompt phase (GRB 990123 (Akerlof et al., 1999), 021211 (Li et al., 2003), GRB 060111B (Klotz et al., 2006)). The former component has been attributed to internal shocks, while the latter was interpreted as reverse shock emission, e.g. Sari & Piran (1999); Mészáros & Rees (1999). The internal shock emission is relativistic, and the timescales in the observer frame are shortened by  $\Gamma^{-2}$ , with  $\Gamma$  being



Table 6.3. *Top 10 brightest optical afterglows of GRBs. Another 19 afterglows reached a maximum brighter than 15 mag in one color.*

GRB	Brightness (mag)	Filter	Time after GRB (sec)	Reference
080319B	3.8	K <sub>s</sub>	65	Bloom et al. (2009)
080319B	5.4	V	53	Racusin et al. (2008)
990123	8.9	white	50	Akerlof et al. (1999)
061007	9.9	white	94	Rykoff et al. (2009)
060117	10.1	R <sub>c</sub>	129	Jelinek et al. (2006)
060418	10.2	K'	168	Molinari et al. (2007)
061126	11.0	K <sub>s</sub>	137	Perley et al. (2008)
081203A	11.6	I <sub>c</sub>	415	West et al. (2008)
081121	11.6	white	60	Yuan & Rujopakarn (2008)
090102	11.8	H	102	Gendre et al. (2010)
030329	11.9	J	8100	Nishihara et al. (2003)

the bulk Lorentz factor which typically is assumed to be of order 300–500. The reverse shock is predicted to happen with little delay with respect to the gamma-ray emission (unless the Lorentz factor is very small), and the corresponding optical emission decays with a power law index of 2 for a constant density environment, or up to 2.8 for a wind density profile (Kobayashi, 2000).

#### 6.4.2 Dark bursts

Originally, those GRBs with X-ray afterglows but without optical detection (about 50%) were coined as “dark GRBs”. The “darkness” in the optical was assumed to be due to one (or more) of several reasons (Fynbo et al., 2001): the afterglow could (i) have an intrinsically low luminosity, e.g., due to a low-density environment or low explosion energy, (ii) be strongly absorbed by intervening material, either very local around the GRB, or along the line-of-sight through the host galaxy, or (iii) be at high redshift ( $z > 6$ ) so that Ly $\alpha$  blanketing and absorption by intervening Lyman-limit systems would prohibit detection in the  $R$  band (most frequently used in the optical). An analysis of a subsample of GRBs, namely those with particularly accurate positions provided with the Soft X-ray Camera on *HETE-2*, showed that optical afterglows were found for 10 out of 11 GRBs (Villasenor et al., 2004). This suggested that the majority of dark GRBs are neither at high redshift nor strongly absorbed, but just faint, i.e., the spread in afterglow brightness at a given time after the GRB is much larger than previous observations

had indicated. However, since 2004 the *Swift* observations have provided a plethora of locations at the few arcsec level within minutes of the GRB, and the fraction of dark bursts is still above  $\sim 30\%$ .

Very recently, a sample with nearly complete afterglow detections was reported, which had been created by selecting those GRBs for which observations with the Gamma-Ray Burst Optical/Near-Infrared Detector *GROND* (operated at the 2.2m telescope at the La Silla Observatory (Greiner et al., 2008)) started within 30 min after the burst (Greiner et al., 2010). With a 95% detection completeness and a simultaneously obtained 7-band spectral energy distribution for all these bursts, rest-frame extinction  $A_V$  is accurately measured for the first time in a coherent way. Substantially more bursts with  $A_V > 0.5$  mag are found than in previous samples Kann et al. (2010), and in many cases a moderate redshift (in the 1–3 range) enhances the effect in the observer frame. The properties of this sample demonstrate that the darkness can be explained by a combination of (i) moderate extinction at moderate redshift, and (ii) a ( $\sim 10\%$ ) fraction of bursts at redshift  $z > 5$ . This strengthens similar earlier suggestions (e.g. Cenko et al., 2009; Perley et al., 2009), which were based on a combination of early detections and host galaxy studies of the non-detected afterglows.

### 6.4.3 Spectral lines

Line detections have been reported at optical and X-ray wavelengths. These early X-ray line detections were based on *BeppoSAX*, *ASCA*, *Chandra* and *XMM-Newton* observations. A comprehensive analysis, however, of  $>200$  *Swift* bursts did not reveal any significant X-ray lines (Romano et al., 2008; Hurkett et al., 2008). Therefore, in the following we will constrain ourselves to optical lines.

Optical/NIR spectroscopy of afterglows usually reveals absorption lines of (typically more than one) system along the line of sight between the GRB and the observer. The system with the largest redshift is then assigned to be the redshift of the GRB. Formally, these absorption redshifts are still a lower limit, but one would have to assume a contrived empty environment if the GRB were at a much larger redshift than the last absorption system and if it would leave no measurable imprint in the spectrum. Moreover, the detection of a Lyman cutoff or (even time-variable) lines from fine-structure levels provide stringent limits. Measurements of the equivalent widths of the absorption features (e.g., Fig. 6.2) allows us to derive column densities of metal lines and neutral hydrogen, as well as the metallicity and dust content along the line of sight. A special case are

absorption lines from fine-structure and other metastable levels of ions such as  $O^o$ ,  $Si^+$  and  $Fe^+$ , which are ubiquitous in GRB-Damped Lyman  $\alpha$  systems (DLAs) (Vreeswijk et al., 2004; Chen et al., 2005; Berger et al., 2006; Prochaska, Chen & Bloom, 2006), and very likely are excited by the GRB emission.

Interestingly, in about half of the cases, the GRB-DLAs exhibit column densities of  $\log(N_H) \sim 10^{22} \text{ cm}^{-2}$  or above (Fynbo et al., 2009). This is in contrast to the only few such systems in QSO-DLAs (Noterdaeme et al., 2008), and is likely due to the smaller range of galactocentric distances probed by GRB sightlines (for a detailed discussion on GRB-DLAs see also Chapter 13).

An interesting puzzle was brought up by Prochter et al. (2006), namely that the number density of strong (equivalent widths  $> 1 \text{ \AA}$ ) intervening MgII absorbers detected in GRB afterglow spectra at redshifts  $0.5 < z < 2$ , is nearly 4 times larger than those in the QSO spectra. Similar analyses based on a different dataset found a factor 2 larger incidence rate (with higher significance than the earlier factor 4), but only for strong absorbers, while for weaker absorbers, (equivalent widths in the  $0.3\text{--}1.0 \text{ \AA}$  range), the incidence rate was consistent with that in QSO spectra (Vergani et al., 2009; Tejos et al., 2009). A similar study with CIV absorbers did not reveal any differences between GRB and QSO sightlines (Sudilovsky et al., 2007). A number of possible explanations have been proposed (Porciani, Viel & Lilly, 2007), including a dust extinction bias, or different beam sizes of the sources, or lensing amplification, but none provided a conclusive solution of this discrepancy so far.

Depending on its brightness, early host spectra might already show emission lines. Usually, host spectroscopy is done when the GRB afterglow has faded away. To date (2010), there has not been a single case of emission lines being at a larger or smaller redshift than the highest-redshift absorption system, supporting the assumption that the GRB belongs to the corresponding host galaxy. Besides giving the redshift, the observed emission lines of OII, [OIII] and the Balmer series are used to infer the global extinction, metallicity and star formation rate (Savaglio et al., 2009; Levesque et al., 2010). Note that in this case these are host-integrated quantities, in contrast to the line-of-sight measurements via absorption lines.

#### 6.4.4 Line Variability

Variability of both absorption and emission lines has been searched for, though on substantially different timescales.

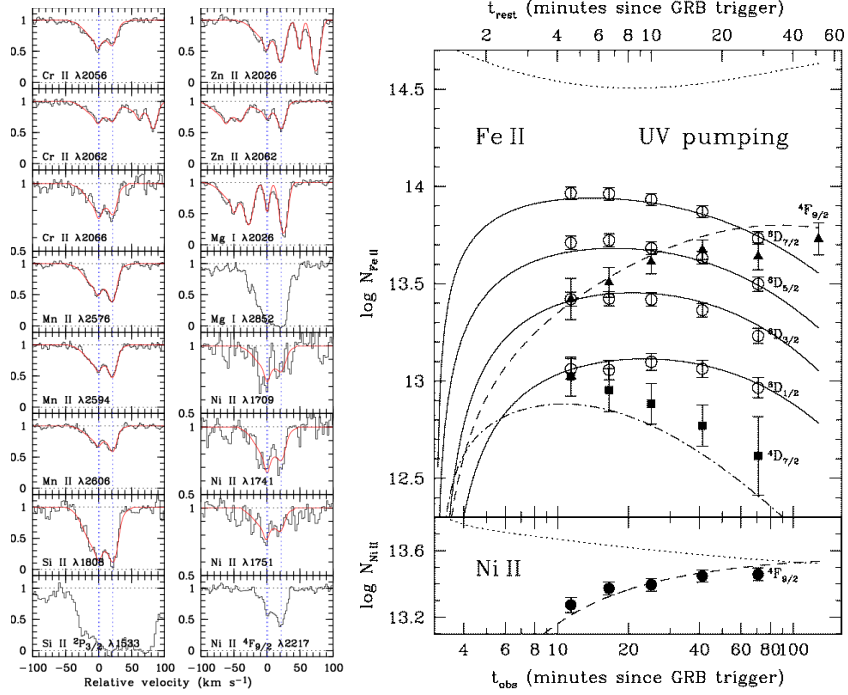


Fig. 6.2. **Left:** Absorption line profiles for a variety of transitions detected at the GRB 060418 redshift. Red lines show the Voigt-profiles fits of low-ionization species. **Right:** Observed total column densities for the fine-structure lines (open circles), the first metastable level (filled triangle) and the second metastable level (filled squares) of FeII (top) and the total column densities for NiII (bottom). Lines are the best-fit UV pumping model. From Vreeswijk et al. (2007)

Variable absorption lines, involving the fine structure of the ground level and other metastable energy levels of  $\text{Fe}^+$  and  $\text{Ni}^+$  were first modelled (Fig. 6.2) for GRBs 020813 and 060418 (Dessauges-Zavadsky et al., 2006; Vreeswijk et al., 2007). It was demonstrated that these lines are formed by UV pumping, i.e. excitation to an upper level due to the absorption of a UV photon, followed by de-excitation cascades, as suggested by Prochaska, Chen & Bloom (2006). This interpretation allowed the first determination of the distance between the GRB and its DLA to an astonishing 1.7 kpc. Later re-modelling with a different set of atomic abundances increased this distance to  $2.0 \pm 0.3$  kpc (Ledoux et al., 2009). For GRB 050730, the same authors derived a distance (near-side of the cloud) of  $440 \pm 30$  pc for a cloud  $520_{-190}^{+240}$  pc size (along the line of sight). This is in contrast to a distance of only about 50–100 pc for which the GRB radiation can ionize hydrogen. The global

picture derived from modelling these variable lines is that of the absorber being a large, diffuse cloud with a broadening parameter and physical size typical of the Galactic ISM, with low metallicity and low dust content, and at a distance at least 0.1–1 kpc away from the GRB (Ledoux et al., 2009).

Variability of the emission lines was expected since the GRB prompt and afterglow emission ionizes its surrounding to substantial distances. Depending on the density of the circumburst medium, this leads to recombination lines over timescales of years which could compete with the emission lines usually assigned to star-formation. In fact, it had been proposed to use the GRB-induced lines for the identification of remnants of GRBs in nearby galaxies (Band & Hartmann, 1992; Perna, Raymond & Loeb, 2000). Such a search was indeed conducted for the host galaxy of GRB 990712, but no variability was found in the OIII [5007] line over a timescale of 6 years (Küpcü Yoldaş et al., 2006).

### 6.4.5 Continuum variability

#### 6.4.5.1 Early lightcurve behaviour

The early time GRB afterglow behaviour depends strongly on the wavelength range considered. At soft X-rays, *Swift* has found surprisingly rapid variability in both, short- and long-duration GRBs. Yet, many of the early light curves show a canonical behaviour with three distinct power law segments (Nousek et al., 2006): a bright, rapidly declining ( $t^{-\alpha}$ , with  $\alpha > 3$ ) emission, which smoothly connects to the prompt emission both temporally and spectrally (Tagliaferri et al., 2005; Barthelmy et al., 2005), followed by a steep-to-shallow transition, which is usually accompanied by a change in the power-law index of the spectrum. The first break has been interpreted (Nousek et al., 2006; Zhang et al., 2006) as the slowly decaying forward shock emission as it becomes dominant over the rapidly declining tail emission of the prompt  $\gamma$ -rays as seen from large angles (Kumar & Panaitescu, 2000). The subsequent shallow phase is commonly interpreted as due to continuous energy injection into the external shock (Nousek et al., 2006; Zhang et al., 2006), which implies that most of the energy in the afterglow shock was either injected at late times after the prompt  $\gamma$ -ray emission, or was originally in slow material that would not have contributed to the prompt emission. This shallow phase then transitions into the late afterglow phase with no clear evidence for a spectral change.

Extended emission lasting about 100 sec has been detected at hard X- and gamma-rays in about 25% of the short bursts (Norris & Bonnell, 2006). Though these tails were known already from *HETE-2* (Villasenor et al.,

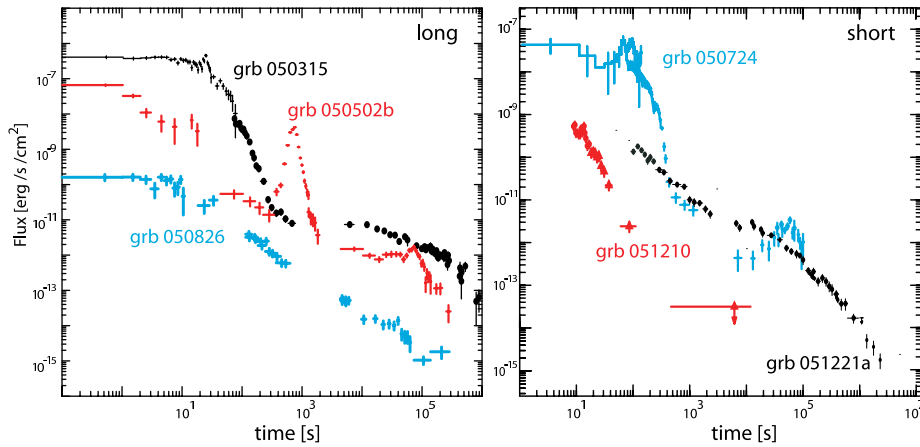


Fig. 6.3. Representative examples of X-ray afterglow light curves of long (left) and short-duration (right) GRBs. From Gehrels, Ramirez-Ruiz & Fox (2009).

2005) and *CGRO*/BATSE (Lazzati, Ramirez-Ruiz & Ghisellini, 2001; Connaughton, 2002; Norris & Bonnell, 2006) a systematic study was only possible with *Swift* (Norris, Gehrels & Scargle, 2010), since this emission is rather soft and has spurred debate on whether it is afterglow or prompt emission.

The optical afterglow behaviour is at least as diverse as the X-ray one (Fig. 6.4): A large fraction of the afterglows show the canonical smooth power law decay, but some show a completely different behaviour. There are rare cases (like GRBs 990123 or 080319B) which are dominated by very bright, fast decaying emission, which is usually interpreted as the appearance of the reverse shock (Akerlof et al. (1999); Racusin et al. (2008); Bloom et al. (2009), but see e.g., Genet & Granot (2009) for an alternative interpretation). About 10–20% of the optical afterglows exhibit an increase in their brightness during the first few hundred seconds. This has been observed both with the *Swift*/ Ultra Violet Optical Telescope (UVOT) (Oates et al., 2009) as well as with fast-slewing telescopes from the ground (Rykoff et al., 2004; Quimby et al., 2006; Yost et al., 2006; Molinari et al., 2007; Krühler et al., 2008; Covino et al., 2008; Krühler et al., 2009). No color evolution, however, was seen during the rise and the turn-over towards decay. The deceleration of the forward shock by the external medium has been favoured as an explanation for light curve shapes, where the rise and subsequent decay can be modelled with a broken power-law. The time of maximum light was also used to derive initial Lorentz factors of 80–300. Cases, where the decay showed another break at early times, and the power-law indices of the rise and first decay did not match the standard fireball prediction, have been in-

terpreted as a signature of jet emission seen off-axis (Panaitescu & Vestrand, 2008). Assuming that the jet structure has a power-law angular distribution, there is a correlation between initial rise time and the slope of the first fading after maximum, which can explain the observed diversity of light curves (Panaitescu & Vestrand, 2008) – though applications to larger samples have not confirmed this trend (Klotz et al., 2009; Kann et al., 2010).

An interesting consistency check is now possible with measurements from *Fermi* and *INTEGRAL*: the Lorentz factor can also be determined from the variability of the gamma-ray emission (Lithwick & Sari, 2001). For GRB 080928 (Rossi et al., 2010) this comparison has been attempted for the first time, and the two values of the initial Lorentz factor are indeed broadly consistent.

#### 6.4.5.2 Jet-breaks

An observer will detect emission due to relativistic beaming of the emission from the GRB blast wave within an angle  $\sim 1/\Gamma$  of the line of sight (see also Chapter 11). The afterglow is thus a signature of the geometry of the ejecta. Until the blast wave has decelerated such that its opening angle is  $\sim 1/\Gamma$ , its gradual fading is partly compensated by an increasing emission region. Only at angles larger than  $1/\Gamma$ , does the observed emission decay with a power-law index of  $>2$  and can be described under a spherically symmetric model. Since this transition is a geometric effect, the slope change in the afterglow light decay should be achromatic (Rhoads, 1999), that is observable at all wavelengths at the same time.

In the pre-*Swift* era, this achromatic steepening was commonly reported in the optical afterglows and interpreted as the indication of beamed emission. Using the pre-*Swift* data, collimation factors of  $\Omega/4\pi \lesssim 0.01$ , corresponding to half opening angles of  $\lesssim 8^\circ$  were derived from the timing of these breaks (Frail et al., 2001; Bloom et al., 2003).

However, with *Swift* only a small fraction of bursts has been reported with convincing evidence for an X-ray jet break (Racusin et al., 2009). Today a general consensus has developed according to which the breaks in *Swift*-detected bursts occur at later times due to their larger mean redshift, and thus at flux levels beyond the sensitivity of standard follow-up campaigns. Recent results of a dedicated long-term monitoring of X-ray afterglows with *Chandra* seems to recover jet breaks for about 40% of the *Chandra* observed bursts (Burrows et al., 2010).

#### 6.4.5.3 X-ray flares

GRB 050502B provided one of the first examples of the dramatic X-ray flaring activity in the early afterglow evolution (Burrows et al., 2005; Falcone et al., 2006). This burst also demonstrated that X-ray flares (measured up to 10 keV) can contain energy comparable to the one emitted during the prompt GRB phase in the 15–300 keV band. Surprisingly, X-ray flares have been seen in long- and short-duration GRBs, as well as at low and high redshifts: even GRB 090423 at  $z \sim 8.2$  exhibited a flare with rather standard properties (Chincarini et al., 2010). The majority of the flares occurs during the first  $10^3$  s after the GRB trigger, but some have also been seen as late as  $10^5$  or even  $10^6$  s (Curran et al., 2008) (see next section). The flares are relatively sharp, with  $\Delta t/t \sim 0.1$ , and are spectrally different (harder) than the underlying afterglow emission. There is considerable spectral evolution during a flare with a hardening during the rise followed by softening during the decay (Goad et al., 2007; Krimm et al., 2007; Godet et al., 2007). The first case where these flares were seen simultaneous in the optical/NIR was GRB 071031 (Krühler et al., 2009), which showed that the peak of the emission shifts at late times from the few keV band into the UV. Given that the flare phenomenology is very analogous to that of the prompt gamma-ray emission, it is now generally accepted that X-ray flares and gamma-ray pulses are produced by the same mechanism.

#### 6.4.5.4 Early time afterglow features (“humps”)

Some GRB afterglows (GRBs 021004, 030329) exhibited “humps” on top of the canonical optical fading at timescales of  $10^4$ – $10^5$  s after the GRB onset (Lazzati et al., 2002; Lipkin et al., 2004). Originally, these humps were interpreted as the interaction of the blast wave with moderate density enhancements in the ambient medium, with a density contrast of order 10 (Lazzati et al., 2002); later models employed additional energy injection episodes (Björnsson, Gudmundsson & Johannesson, 2004). Optical afterglow variability due to the interaction with the ISM is not expected later than  $10^6$  s because the blast wave, once it has swept up enough interstellar material to produce the canonical afterglow emission, is thought to be only mildly relativistic. It is possible, but not easy to prove due to lacking X-ray observations, that these humps are related to the X-ray flares discussed in the previous section.

#### 6.4.5.5 Late afterglow features: Supernovae and something else?

There is now general consensus that the long/soft (Kouveliotou et al., 1993) GRBs are intimately connected to the deaths of massive stars. About 70%



of core-collapse supernovae (SNe) are those of type II; one of the peculiar sub-classes that form part of the other 30% are type Ib/c supernovae.

While the supernova-GRB connection was proposed some years ago (Galama et al., 1998a; Iwamoto et al., 1998), the unambiguous spectroscopic identification of the lowest-redshift long-duration GRBs as supernovae during the last decade provided convincing evidence for this association (Hjorth et al., 2003; Stanek et al., 2003) (Fig. 6.5). The supernovae in the five spectroscopically confirmed gamma-ray bursts (GRB 980425/SN 1998bw, 030329/2003dh, 031203/2003lw, 060218/2006aj and 100316D/2010bh) are all of type Ic, with unusually large kinetic energy (very large expansion velocities of order 10–30 thousand km/s were measured after 10 days) and ejected mass of radioactive  $^{56}\text{Ni}$ ; such SNe were called hypernovae by Paczynski 1998. Their latter property in particular suggests progenitors with masses  $\gtrsim 40 M_{\odot}$  (Nomoto et al., 2004), though the detailed analysis of the light curve and spectra of GRB 060218 / SN 2006aj showed that the initial mass was only  $\sim 20 M_{\odot}$ , indicating a possibly broader range of progenitor masses leading to a GRB (Mazzali et al., 2006). Theoretically, SNe Ib/c are favoured over type II because the former have typically smaller envelope masses, and are thus thought to allow easier break-out of the GRB jet. Moreover, the lack of hydrogen lines in the GRB afterglow spectra is consistent with the collapsar model, where the progenitor star lost its hydrogen envelope to become a Wolf-Rayet star before collapsing.

In contrast to these relatively similar spectroscopic properties among the GRB-SN, the  $\gamma$ -ray emission properties of the corresponding GRBs differ in their total emitted energy (Kaneko et al., 2007), temporal profile and spectral shape, implying that the  $\gamma$ -ray properties are not determined by the progenitor mass, but most likely by completely different properties (Gal-Yam et al., 2006a).

Two noteworthy exceptions to this picture of SNe detections associated with the nearest bursts are GRB 060505 and 060614. A host galaxy at  $z=0.125$  was associated with this burst based on two optical emission lines; moreover this was clearly a long-duration burst ( $T_{90}=102$  s). However, no SN was found in the error box of GRB 060614 (Fynbo et al., 2006; Della Valle et al., 2006) to limits about a factor 100 fainter than previous detections. Both bursts have spurred extensive discussions on the homogeneity of the class of GRB-SN, and the classification of GRBs (Gal-Yam et al., 2006a; Gehrels et al., 2006; Zhang et al., 2009). Gehrels et al. (2006) proposed a third parameter for GRB classification based on their spectral lags (difference of arrival times between high and low-energy photons) and their peak luminosities. Accord-

ing to this criterion, the spectral lag of GRB 060614 would place this burst entirely within the short-duration GRB subclass (Gehrels et al., 2006).

Finally, a number of GRBs show optical humps at late times, but earlier than the expected appearances of their related SNe, around  $10^5 - 10^6$  s (McBreen et al., 2010). Multi-color light curves show that these humps are achromatic, excluding very early SNe. The cause of these humps is still a matter of debate.

#### 6.4.5.6 *Very late afterglow evolution*

The expansion of GRB afterglows, while being initially ultra-relativistic, slows down in the course of time and eventually enters a sub-relativistic phase after several tens to hundreds of days. With the notable exception of GRB 060729 (Grupe et al., 2010), most afterglows are too faint to be detectable in most wavelengths at such late times, and their observations are confined mainly to low-frequency radio bands. Despite a large number of afterglow detections at radio wavelengths (see, e.g. Frail et al., 2003a), only two well studied examples exist so far of observations, in multiple radio bands, deep into the non-relativistic phase: GRB 970508 and GRB 030329. For the former, radio follow-up at the 1.4 GHz to 8.4 GHz range was conducted for more than 400 days post-burst, while the transition to non-relativistic expansion occurred at  $\sim 100$  days (Frail, Waxman & Kulkarni, 2000). In the case of GRB 030329, radio observations at several frequencies, (610 MHz to 4.8 GHz) over  $\sim 1200$  days after the burst have been reported (Van der Horst et al., 2008) The non-relativistic transition time in this case was estimated to be  $\sim 60 - 80$  days.

Observations well within the non-relativistic phase provide a useful additional tool to derive the physical parameters of the burst, in particular the total (bolometric) energy (Oren, Nakar & Piran, 2005; Kaneko et al., 2007). The dynamics in this regime is governed by the Sedov-Taylor solution, which is different from the Blandford-McKee solution in the early relativistic phase before the jet break. Burst parameters derived from the non-relativistic phase alone may, therefore, be considered as a set of independent measurements, which serve as a useful check on the quantities derived from the relativistic phase evolution. Multiband modelling of the relativistic phase needs to include a description of the angular distribution of the energy and Lorentz factor of the outflow, which remains uncertain even in the presence of a well-determined jet break. In the deep non-relativistic phase, however, the expansion of the blast wave is expected to have become nearly isotropic, so the energy estimates are much less prone to uncertainties arising from collimation effects. The total energy

$E_{\text{ST}}$  estimated for the Sedov-Taylor non-relativistic phase, together with the isotropic equivalent energy  $E_{\text{iso}}$  estimated from burst fluence and relativistic phase modelling, provide a useful indicator of the degree of initial collimation of the relativistic outflow. In the case of GRB 970508 the estimated values of  $E_{\text{ST}}$  and  $E_{\text{iso}}$  are  $\sim 5 \times 10^{50}$  erg and  $\sim 10^{52}$  erg, respectively, suggesting an initial collimation angle  $\leq 20^\circ$  (Frail, Waxman & Kulkarni, 2000). For GRB 030329, the corresponding estimates are  $\sim 8 \times 10^{50}$  erg and  $\sim 7 - 8 \times 10^{51}$  erg, respectively (Berger, Kulkarni & Frail, 2004; Frail et al., 2005; Van der Horst et al., 2008).

Several microphysical quantities may in fact be a function of the dynamical regime, and hence may not have the same value in the relativistic and the non-relativistic phase. These may include parameters such as  $\epsilon_e$ , the fraction of the total energy resident in relativistic electrons,  $\epsilon_B$ , the fraction of the total energy resident in post-shock magnetic field, and  $p$ , the power-law index of the electron energy distribution. By modelling the relativistic and the non-relativistic phase evolution separately, one may in principle be able to conclude whether these microphysical parameters are indeed different in the two phases. Obtaining a complete solution for physical parameters in the non-relativistic phase requires the measurement of all three spectral breaks,  $\nu_a$ ,  $\nu_m$  and  $\nu_c$ . Multi-band radio light curves can be used to determine the first two of these breaks, but a direct measurement of the cooling frequency in the non-relativistic phase has not yet been possible, in the absence of high frequency observations. As an approximate estimate, one uses the value of  $\nu_c$  extrapolated from an earlier, relativistic phase to infer the physical parameters.

Because of this partial lack of information and also the uncertainties inherent in the measurement of spectral parameters, it is not yet possible to state with confidence whether the microphysical parameters are indeed different between the relativistic and the non-relativistic phase. Nevertheless, in both GRB 970508 and in GRB 030329 one finds that in the non-relativistic phase the energy in relativistic electrons and that in the magnetic field are nearly in equipartition (Frail, Waxman & Kulkarni, 2000; Van der Horst et al., 2008), while in the relativistic phase the derived estimates of  $\epsilon_B$  tend to be significantly smaller than those of  $\epsilon_e$  (see, e.g. Panaitescu & Kumar, 2001, 2002).

Another important measurement that is made possible by the long-lasting radio follow-up of an afterglow is that of the expansion rate of the blast wave. In the case of GRB 970508 an apparent superluminal transverse expansion was inferred from the evolution of the modulation index of the scintillating flux at 8.5 GHz (Frail et al., 1997). Early in the evolution, the radio

flux showed significant fluctuations (up to  $\sim 50\%$ ), as would be expected due to interstellar scintillation of a source of very small angular size. This scintillation gradually decreased with time, and became nearly imperceptible after  $\sim 50$  days. This evolution can be attributed to an increase of the angular size of the source with time. The expansion rate derived from these observations was  $\sim 3 \mu\text{as}$  in  $\sim 2$  weeks, which, at the redshift of the source ( $z=0.835$ ), amounted to a transverse expansion speed of  $\sim 4$  times the speed of light. Using the standard interpretation of superluminal motion, this would suggest that the average bulk Lorentz factor of the blast wave  $\sim 2$  weeks after the burst was  $\sim 4$  (Frail et al., 1997).

In the case of GRB 030329 it has been possible to directly measure the angular extent of the expanding source using Very Long Baseline Interferometry (VLBI) at several epochs over nearly 3 years following the burst (Taylor et al., 2004; Pihlström et al., 2007). These measurements show an apparent superluminal transverse expansion rate in the early phase ( $v \sim 6c$  at  $\sim 20$  days after burst), which gradually becomes sub-luminal around  $\sim 1$  yr after the burst. The evolution of the apparent transverse size can be used to distinguish between several possible models of post jet-break lateral expansion of the blast wave – the available measurements on GRB 030329, however, are not strongly constraining in this regard (Granot, Ramirez-Ruiz & Loeb, 2005; Pihlström et al., 2007). The non-relativistic transition time derived from the VLBI measurements of GRB 030329 appear to be a factor of  $\sim 2$  larger than that required to successfully model the multi-wavelength light curves of the afterglow (Pihlström et al., 2007; Van der Horst et al., 2008). The reason for this discrepancy is yet to be fully understood.

#### **6.4.6 Polarization**

One direct consequence of synchrotron emission is that the emission from an individual particle is polarized. Due to the probably random nature of the post-shock magnetic fields, the polarization is likely to be averaged out and only a small degree will be left. The time at which linear polarization is detectable is thought to be around the jet-break time. Several (differing) models have been proposed, in which a collimated jet and an off-axis line of sight conspire to produce an asymmetry which leads to net polarization including one or several  $90^\circ$  changes of the polarization angle (Ghisellini & Lazzati, 1999; Sari, 1999). This behaviour could provide independent evidence for the jet structure of the relativistic outflow.

The observed polarization at optical wavelengths at later times is less than  $3\%$  (Hjorth et al., 1999; Wijers et al., 1999; Rol et al., 2000) with one,

debated, exception of 10% (Bersier et al., 2003). Because of these low-levels and the rapid decline of the afterglow brightness during the first day, it has been difficult to observe changes in the polarization as predicted by theory. The by far most extensive observations of a light curve with fast variability in polarization degree and angle (Fig. 6.6) have been obtained for the afterglow of GRB 030329 (Greiner et al., 2003). This variability pattern does not follow any of the model predictions, and is also not correlated with brightness. The global behaviour is consistent with the interpretation that the GRB is emitted in a relativistic jet with an initial opening angle of  $3^\circ$ . However, in this GRB afterglow several re-brightenings superposed to a power-law decline have likely caused deviations from a simple single-jet model, thus making it difficult to interpret. The low level of polarization implies that the components of the magnetic field parallel and perpendicular to the shock do not differ by more than  $\sim 10\%$ , and suggests an entangled magnetic field, probably amplified by turbulence behind shocks, rather than a pre-existing field.

Very recently, an optical polarization measurement of GRB 090102 was achieved at a time when the reverse shock emission was dominating the light curve (Steele et al., 2010). The method uses a rotating polaroid which allows simultaneous measurements of the polarization degree of neighbouring stars but not the angle. This implies that the constant polarization of the Galactic foreground ISM could not be subtracted, and thus the measured polarization of  $10.2 \pm 1.3\%$ , is likely an upper limit. This relatively high level has been interpreted as evidence for the presence of large-scale ordered magnetic fields in the relativistic outflow. In the present case, the magnetisation, i.e., the ratio of magnetic to kinetic energy, must have been fine-tuned to near 1. Any value substantially larger than 1 would suppress the observed reverse shock, while values well below 1 would not produce a net polarization at the measured level.

#### 6.4.7 Orphan afterglows

An exciting consequence of beaming is that there should exist GRBs which develop a less beamed X-ray, optical, or radio afterglow, but for which we miss the prompt GRB emission - the so-called orphan (Fig. 6.7) afterglow (for a discussion see, e.g., Rhoads (1997); Mészáros, Rees & Wijers (1998); Perna & Loeb (1998)). Archival X-ray data have been searched for such events, but none was found (Grindlay, 1999; Greiner et al., 2000). In the optical, a small number of dedicated surveys was performed; there no candidate event was found in 125 hrs of monitoring of a field of 256 sq.

deg. with *ROTSE-I* to a limiting magnitude of 15.7 (Kehoe et al., 2002). Vanden Berk et al. (2002) searched for color-selected transients within 1500 sq. deg. of the Sloan Digital Sky Survey (*SDSS*) down to  $R = 19$  and found only one unusual transient which was later identified as a radio-loud AGN exhibiting strong variability (Gal-Yam et al., 2002). A couple of interesting optical transients were found in the  $B$ ,  $V$  and  $R$ -band Deep Lens Survey (*DLS*) transient search, within an area of  $0.01 \text{ deg}^{-2} \text{ yr}^{-1}$  with a limiting magnitude of 24. None of these could be positively associated with a GRB afterglow (Becker et al., 2004) and all were later shown to have been flares from M dwarfs in our Galaxy (Kulkarni & Rau, 2006). In another unsuccessful search using the *ROTSE-III* telescope array (Rykoff et al., 2005) placed an upper limit on the rate of fading optical transients with quiescent counterparts dimmer than  $\sim 20$ th magnitude of less than  $1.9 \text{ deg}^{-2} \text{ yr}^{-1}$ . Finally, a monitoring project of  $\sim 12$  sq. deg. in 25 nights (at a typical spacing of 2 nights) down to a limiting magnitude of  $R \sim 23$  mag found no afterglow candidate, providing a limit on the collimation factor (ratio of the true rate of on-axis optical afterglows to long-duration GRBs which produce observable optical afterglows) of  $< 12\,500$  (Rau, Schwarz & Greiner, 2006).

In the radio band, orphan afterglows have been searched for by combining the Faint Images of the Radio Sky at Twenty-centimeters (*FIRST*) and the NRAO VLA Sky Survey (*NVSS*), with the result of finding 9 afterglow candidates and implying a limit on the beaming factor of  $f_b^{-1} \equiv (\theta^2/2) > 13$  if all candidates, and  $f_b^{-1} > 90$  if none are associated with GRBs, respectively (Levinson et al., 2002). These authors also noted the, at first glance anti-intuitive, fact that the number of orphan radio afterglows is smaller for smaller jet opening angles in a flux-limited survey (for narrower beams each GRB has a lower energy and, therefore, is more difficult to detect) Later, Gal-Yam et al. (2006b) concluded that none of the transient objects was an orphan afterglow and set an upper limit for the beaming factor,  $f_b^{-1} > 62$ . Recently, there is evidence for an orphan radio afterglow found in the search for type Ibc SNe, through the discovery of luminous radio emission from the seemingly ordinary type Ibc SN 2009bb, which, however, requires a substantially relativistic outflow powered by a central engine (Soderberg et al., 2010). A mildly relativistic outflow was also observed in SN 2007gr (Paragi et al., 2010). These detections indicate that, most likely, the relativistic energy content of Ibc SNe varies dramatically, while their total explosion energy maybe more standard.

## 6.5 Constraints from multi-wavelength afterglow observations

### 6.5.1 Fireball parameters

The evolution of the blast wave in the fireball model is governed by the total energy in the shock, the geometry of the outflow, and the density structure of the ISM into which it is expanding (see also Chapters 7 and 8). The time dependence of the radiated emission depends on the hydrodynamic evolution and the distribution of energy between electrons and magnetic field (Sari & Piran, 1999). Unfortunately, only for few bursts sufficient data have been collected in order to derive the fundamental physical parameters: GRBs 970508 (Fig. 6.8) (Galama et al., 1998b; Wijers & Galama, 1999), 980329 (Yost et al., 2002), 980703 (Frail et al., 2003b) and 051111 (Butler et al., 2006).

Despite this sparse number of GRBs sampled, it is obvious that the diversity in physical parameters is large: the ISM density ranges between  $0.1\text{--}500\text{ cm}^{-3}$ , total energies are  $10^{51}$  to  $10^{53}$  erg, and the energy distribution between electrons and magnetic field is consistent with equipartition. Future observations are clearly warranted to improve our understanding of the distributions in these parameters, and to what extent more sophisticated models with more parameters are needed.

### 6.5.2 Environment

#### 6.5.2.1 Extinction

Besides deriving the fireball parameters from spectral energy distributions (SED), emphasis has also been given to the curvature of broad-band spectra in the optical/near-infrared (NIR) region due to dust extinction, and in the soft X-ray band due to absorption by gas.

Effective neutral hydrogen absorption in excess of the Galactic foreground absorption has taken a long way to get detected significantly in GRB afterglow spectra. Originally not detected at all in the full sample of BeppoSAX bursts (De Pasquale et al., 2003), a re-analysis of the brightest 13 X-ray afterglows revealed statistically significant absorption in excess of the Galactic one for two bursts (Stratta et al., 2004). Already 8 bursts of 17 observed with *Chandra* or *XMM-Newton* until Oct. 2004 show excess absorption (Gendre et al., 2006). In the Swift era, excess absorption is detected in the majority of bursts, in selected samples up to 85% (Greiner et al., 2010).

In the optical/NIR, extinction measurements for a long time have been hampered by the lack of proper SED measurements, and the interrelation of spectral slope, redshift and extinction. Early attempts therefore concen-

trated on deep NIR observations (e.g. Klose et al., 2003). In a first systematic way (Kann et al., 2006) collected photometry of 19 bursts from the literature, constructed light curves, shifted measurements of different filters to a common epoch according to the light curve, and derived spectral slope and extinction  $A_V$ . While little evidence was found for substantial  $A_V$ , the prevalence of a SMC-like dust extinction curve was noted. In the Swift era, UVOT observations provided more accurate  $A_V$  measurements, but for a sample which is strongly biased towards bright and small- $A_V$  bursts (Schady et al., 2007, 2010). Recently, the systematic GRB follow-up with the P60 (Cenko et al., 2006) and GROND instruments (Greiner et al., 2008) provided the first unbiased view on the extinction properties (see section 6.4.2), with a substantially larger fraction of bursts with moderate  $A_V$  (Cenko et al., 2009; Greiner et al., 2010).

#### 6.5.2.2 Wind vs. constant density profile

The likely progenitor of long-duration GRBs is the stripped core of a massive star of initial mass  $\gtrsim 25 M_\odot$ , similar to a Wolf-Rayet star. The winds from these stars in our Galaxy have velocities of 1000–2500 km/s and mass-loss rates of  $10^{-5} - 10^{-4} M_\odot/\text{yr}$ . Before exploding and creating a GRB, a Wolf-Rayet star is thus expected to be surrounded by a medium with density  $\rho \propto r^{-s}$ , where  $r$  is the distance from the star, and  $s=2$  for a stellar wind density profile and  $s=0$  for a constant interstellar medium (ISM) density.

The emission for a thin shell model expanding into a pre-blown wind has been calculated by Chevalier & Li (1999, 2000), while that interacting with a constant ISM density ( $s=0$ ) can be found in Waxman (1997); Sari, Piran & Narayan (1998). The appearance of the spectrum (as determined by the power law index  $p$  of the electron distribution) at a given time is similar for both cases, but the evolution is different. At high frequency, e.g., optical/X-rays, for  $s=0$  the flux evolution goes from adiabatic ( $\propto t^{-(3p-3)4}$ ) to cooling ( $\propto t^{-(3p-2)4}$ ) while for  $s=2$  it goes from cooling ( $\propto t^{-(3p-2)4}$ ) to adiabatic ( $\propto t^{-(3p-1)4}$ ). While cooling, the two cases have the same spectrum and decline. At low frequency (radio), the flux evolution is  $\propto t^{1/2}$  for  $s=0$ , but can make a transition from  $\propto t$  to constant for  $s=2$  (Chevalier & Li, 1999).

Although wind models are indicated for some observed afterglows, the majority are better described by constant density environments.



### 6.5.3 Progenitors

#### 6.5.3.1 Long-duration GRBs

Based on the observed supernova connection (Woosley & Bloom, 2006), the progenitors of long-duration GRBs are intimately connected to supernovae. These progenitors must have lost their hydrogen envelope prior to the supernova explosion. In order to explain the observed statistics, the progenitors must be massive and frequent enough: A comparison of the supernova features in GRB afterglow light curves with those of non-GRB related stripped-envelope supernovae shows that the GRB-SN have, on average, considerably higher kinetic energies and ejected masses (Richardson, 2009). Which special circumstances lead to the final occurrence of a GRB is not fully understood. There are certain mass ranges which make an explosion more difficult, but this depends on the rotation of the progenitor (Fryer, 1999; Woosley, Heger & Weaver, 2002). Also, besides single star channels also binary channels have been proposed (e.g. Smartt et al., 2002; Podsiadlowski et al., 2004; Fryer & Heger, 2005), making a specific prediction difficult.

The role of rotation in supernovae is a long-standing question going back to Hoyle (1946), but for GRB-SN there is general consensus that rotation is required. However, the details (Heger, Langer & Woosley, 2000; Spruit, 2002) as well as the questions of binarity (Yoon & Langer, 2005) remain open. The rotation as well as the mass of the GRB progenitor are crucially influenced by mass loss. Replenishment of material lost from the surface will reduce the rotation rate, and mass loss will make the star lighter at the time of explosion.

Preferred GRB scenarios thus have a small mass-loss rate, particularly in the Wolf-Rayet phase, at which the mass loss rate is smaller for low metallicity (Vink & de Koter, 2005). This has led to the general expectation that GRBs should favour low metallicity regions (MacFadyen & Woosley, 1999).

The above line of thoughts might suggest that high-redshift bursts should have, in general, longer duration than nearby bursts. Lower metallicity in the early phases of the Universe would leave more mass and rotation energy with the progenitor due to less strong winds, which in turn should have a consequence on the time scale of accretion and/or fall-back. With the present sample of GRBs with redshift no such correlation is seen (Fig. 6.9), indicating that the duration measure  $T_{90}$  does not (only) depend on mass and rotation.

An interesting point, however, is that a fraction of  $\sim 8\%$  of long-duration

bursts have rest-frame durations  $\lesssim 1$  sec (independent of redshift; see Fig. 6.9). This poses the question of how massive stars can produce burst of such short duration? Since the fall-back of material from the envelope is of order 100 sec, this high rate of intrinsically short bursts related to massive stars may imply that the burst duration is rather determined by the ejection of the jet or the dissipation of the kinetic energy of the jet.

Population synthesis models show that for the redshift range 6–10 the majority of GRB progenitors are Population II stars (Belczynski et al., 2010), as Population III (metal free) stars have already finished their evolution and Population I (metal rich) stars are just beginning to form. The peak of the long-duration GRB rate depends on the poorly constrained metallicity evolution and peaks at  $z \sim 7$  (3) for efficient/fast (inefficient/slow) mixing of metals (Belczynski et al., 2010).

#### 6.5.3.2 Short-duration GRBs

The association of short GRBs with early-type galaxies (Gehrels et al., 2005; Bloom et al., 2006), and the burst localizations being relatively distant from the center of the host, have supported the earlier conjecture that the progenitors of short GRBs are related to an old stellar population, namely binary systems composed of two compact objects that merge after their orbit has decayed through gravitational wave emission (Eichler et al., 1989).

Interestingly, however, some short GRBs are associated with small, star-forming galaxies, and explode close to their center (Troja et al., 2008). In a recent census actually  $4\times$  more bursts reside in star-forming galaxies than in elliptical galaxies (Berger, 2009). This association spurred discussion on different families of progenitors for short GRBs, including different compact object types (Belczynski et al., 2006), proto-magnetars (Metzger et al., 2008), or a tighter connection to the star-formation evolution similar to long-duration bursts (Virgili et al., 2010). A comparison of the luminosities, star formation rates and metallicities of a sample of hosts of short and of long-duration bursts shows, however, that short burst hosts appear to be drawn uniformly from the underlying field galaxy distribution. This suggests a wide age distribution of several Gyr for the progenitors of short GRBs (Berger, 2009), though this is also consistent with the possibility that the associations of short GRBs to host galaxies are systematically flawed.

#### 6.5.4 Jet opening angle

As described above, orphan afterglow searches have not yet been sensitive enough to constrain the beaming fraction in a sensible way. Similarly, po-

larisation measurements have not (yet) confirmed that breaks seen in light curves are jet breaks. Thus, estimates of jet opening angles rely exclusively on the identification of observed breaks in the afterglow light curves, and their association with a jet break. In the HETE-II and BeppoSAX era, the requirement of achromaticity was only loosely applied, due to the sparse coverage of radio, optical/NIR and/or X-ray measurements (Frail et al., 2001; Bloom et al., 2003). These first attempts found the surprising result that the seemingly most energetic bursts also had the smallest beaming factor, so that the true, beaming corrected energy release was strongly clustered.

In the Swift era, measuring the jet opening angle has been a more challenging task: the much better database of X-ray and optical/NIR follow-up of Swift bursts has made identifying achromatic breaks much more rare (Racusin et al., 2009). In the few clear cases, the distribution of jet break times ranges from a few hours to a few weeks with a median of  $\sim 1$  day (Racusin et al., 2009), implying opening angles of few to about  $20^\circ$ . Another uncertainty, which already plagued the first attempts, is the problem of constant ISM or wind density profile, leading to opening angle estimates differing by up to a factor of 2.

With knowledge of the jet opening angle, an estimate of the true rate of GRBs can also be made. In the Universe, there are about 5 supernovae per second (Madau, Della Valle & Panagia, 1998). The exposure and sky-coverage rate corrected GRB rate is about 3 per day. Correcting this for a mean beaming factor of 300 implies that throughout the Universe, the GRB rate is only about 0.2% of the SN rate, and thus a rare phenomenon among core-collapse SNe. If the GRB rate is strongly dependent on metallicity, this fraction will be higher at large redshift.

### 6.5.5 Distance and Energetics

Beyond the prompt emission fluence, two observables are required to determine the energetics of gamma-ray bursts: their distance, and their jet opening angles. Since the discovery of afterglows, redshifts have been measured for nearly 200 bursts (Fig. 6.10); their isotropic equivalent energy is in the range of  $10^{51}$  to  $10^{54}$  erg. However, with only a few jet opening angles measured, the distribution of beaming-corrected energetics remains poorly constrained.

For a handful of bursts detected recently with *Fermi* in the 0.1–several GeV range, light curve breaks or limits could be derived, and beaming-corrected energies determined. Four of these bursts, namely GRB 080916C, 090902B, 090926A and 090323, have beaming-corrected energies  $E_\gamma$  of  $>2\text{-}5$

$\times 10^{52}$  erg (Greiner et al., 2009a; McBreen et al., 2010; Cenko et al., 2010b; Rau et al., 2010), among the highest ever measured. Interestingly, their jet opening angles are not particularly narrow. Values in excess of  $10^{52}$  erg have been reported for another *Fermi*/Large Area Telescope (LAT) detected burst (Greiner et al., 2009a) and a number of *Swift* bursts (Cenko et al., 2010a). These results indicate that the distribution of  $E_\gamma$  is broad (at least a factor of 30) and not compatible with a standard candle (Frail et al., 2001; Bloom et al., 2003). Furthermore, while being compatible with the Amati ( $E_{\text{peak}} - E_{\text{iso}}$ ) relation at the  $2\sigma$  level (Amati et al., 2009), these very luminous GRBs with high values of  $E_{\text{peak}}$  are not compatible with the  $E_{\text{peak}} - E_\gamma$  relationship (Ghirlanda, Ghisellini & Lazzati, 2004). Both these correlations are heuristic, based on prompt gamma-ray emission properties, and have survived over the last decade with measurements by various instruments.  $E_\gamma$  is the beaming-corrected version of  $E_{\text{iso}}$ , the total bolometric energy released by a burst (see chapter ???).

GRBs being beamed, not only the energy per burst is reduced by 2-3 orders of magnitude, but also their frequency is increased correspondingly since an observer will miss most of the narrow-beamed events. This in turn has implications on the GRB rate, and its relation to the star-formation rate.

### 6.5.6 Cosmology

GRB afterglows are bright enough to be used as pathfinders into the very early universe, independent of whether or not the GRB and/or afterglow phenomenon is fully understood.

In contrast to stationary sources at high redshift, GRB afterglows do not appear substantially fainter at increasing  $z$ . Relativistic time dilation implies that the observations of GRBs at the same time  $\Delta t$  after the GRB event in the observers frame (*on Earth*) will be observed at different times in the source frame, e.g. at *earlier* times for more distant GRB. At this *earlier* time the GRB is intrinsically brighter, thus partly compensating the larger distance.

While it seems unlikely that GRBs will soon be used to derive an accurate Hubble-diagram and to constrain cosmological parameters below the accuracy provided by other methods, there are a few other implications of high- $z$  GRB studies for cosmology:

- Since long-duration GRBs are related to the death of massive stars, it is likely that high- $z$  GRBs exist, as exemplified by the recent discoveries of

GRBs at redshift 6.7 (Greiner et al., 2009b) and 8.2 (Tanvir et al., 2009; Salvaterra et al., 2009). Theoretical predictions range between a few up to 50% of all GRBs being at  $z > 5$  (Schmidt, 2000; Lamb & Reichart, 2001; Bromm & Loeb, 2002), while observations indicate a level of 5% (see also Chapter 14). With WMAP data and theoretical expectations pointing towards the first star-formation occurring at  $z \sim 20 - 30$  (Kogut et al., 2003), further redshift records can be expected in the near future. Hopefully, also the spectroscopic follow-up will be improved, thus allowing us to use these high- $z$  bursts to expand our understanding of the early Universe with respect to metallicity evolution or re-ionization history.

- WMAP data also suggest that the onset of re-ionisation happened at  $z = 11 - 20$  (Kogut et al., 2003). Because WMAP only provides an integral constraint on the re-ionisation history of the universe, it has led to the speculation that re-ionisation was either an extended process or happened more than once. Since the intrinsic luminosity as well as the number density of quasars are expected to fade rapidly beyond  $z \sim 6$ , only GRBs are suitable to be used as bright beacons to illuminate the end of the dark age (Barkana & Loeb, 2001; Loeb & Barkana, 2001; Miralda-Escudé, 2003), and potentially allow us to probe the re-ionisation history of the early Universe (Inoue, Yamazaki & Nakamura, 2003).
- Extensive monitoring of afterglows would help to constrain their local environment, and could allow us to tell whether GRB afterglows are decelerated by the intergalactic medium with an increasingly higher density at higher redshift, or by a stratified constant density medium in a bubble cleared by the progenitor star (Gou et al., 2004).
- Studying the distribution and absorption line properties of GRB host galaxies would shed light onto the cosmological structure formation and star forming history (Mao & Mo, 1998).

## 6.6 Prospects for the future

With the launch of Fermi, the GRB field has entered a new era as emphasis is re-directed again to the main emission mechanism. Yet, there are at least two aspects which relate to the afterglow phenomenon: First, the origin of the delayed GeV emission has been proposed to be afterglow emission (e.g. Ghirlanda, Ghisellini & Nava, 2010). Second, it turns out that the very energetic Fermi/LAT bursts are also those with particularly large beaming corrected energies (McBreen et al., 2010; Cenko et al., 2010b).

One might also hope that if GBM positions could be freed of their systematic errors of 5–12 degrees (Briggs et al., 2009), the recovery of optical

afterglows of bright GBM bursts may have a large impact on the question of jet breaks, and consequently on the beaming angle distribution.

Current and near-future improvements in our ground-based facilities include

- the routine use of a spectrograph with a wide wavelength coverage from the atmosphere cut-off to the near-infrared (X-Shooter) at the ESO/VLT, allowing the detection of absorption and emission lines over the full wavelength range accessible from ground.
- the upgrade of the VLA to substantially higher sensitivity (EVLA), and the starting operation of LOFAR and ALMA, the latter covering the peak of the synchrotron spectrum of GRB afterglows, allowing a substantial fraction of, if not all, afterglows to be detected and calorimetry to be used to determine the GRB energetics;
- the upgrades of air Cerenkov telescopes to lower energy thresholds will allow us to cover a larger distance range before photon-photon interactions attenuate the signal.

These instruments will change the number of afterglow discoveries and the amount of data per afterglow dramatically, thus allowing completely new studies to be performed.

In the field of non-electromagnetic signatures, both neutrino and gravitational wave detectors are getting close to the expected fluxes from GRBs. IceCube (Abbasi et al., 2010) and ANTARES (Bouwhuis et al., 2010) should soon be able to detect the typically 1-10 GeV neutrinos which are expected to be produced in the shocks related to GRBs, or even inelastic proton-neutron collisions in shock-free environments, and thus would confirm that protons are accelerated. Similarly, the Advanced LIGO interferometer, once coming online around 2014, should detect of order 10 neutron star mergers related to short GRBs, up to distances of 200 Mpc (Guetta & Stella, 2009), and could provide insight into the inner engine.

**Acknowledgements:** I thank Dipankar Bhattacharya for writing section 6.4.5.6 and Evert Rol for discussions during the early stage of this review. I acknowledge S. Klose and A. Rau for comments on an earlier version of this manuscript, and D.A. Kann for help in preparing Tab. 6.3 as well as a proof reading of the manuscript.

## References

- Abbasi R., Abdou Y., Abu-Zayyad T. et al. (2010). *ApJ* **710**, 346.  
 Akerlof C., Balsano R., Barthelmy S., et al.. (1999). *Nat.* **398**, 400.

- Amati L., Frontera F., Guidorzi C. (2009). *A&A* **508**, 173.
- Band, D. L. & Hartmann, D.H. (1992). *ApJ* **386**, 299.
- Barkana R., Loeb A. (2001). *Phys. Rep.* **349**, 125.
- Barthelmy S.D., Butterworth P.S., Cline T.L. et al. (1996). In: *Gamma-Ray Bursts*, Eds. C. Kouveliotou et al., AIP **384**, p. 580.
- Barthelmy S.D., Cannizzo, J.K., Gehrels, N. et al. (2005). *ApJ* **635**, L133.
- Becker A.C., Wittman D.M., Broeshaar P.C., et al. (2004). *ApJ* **611**, 418.
- Belczynski K., Perna R., Bulik T. et al. (2006). *ApJ* **648**, 1110.
- Belczynski K., Holz D.E., Fryer C.L. et al. (2010). *ApJ* **708**, 117.
- Berger, E., Kulkarni, S.R., Frail, D.A. (2004). *ApJ* **612**, 966.
- Berger E., Penprase B.E., Cenko S.B. et al. (2006). *ApJ* **642**, 979.
- Berger, E. (2009). *ApJ* **690**, 231.
- Bersier, D., et al. (2003). *ApJ* **583**, L63.
- Björnsson G., Gudmundsson E.H., Johannesson G. (2004). *ApJ* **615**, L77.
- Blake C.H., Bloom J.S., Starr D.L., et al. (2005). *Nat.* **435**, 181.
- Bloom J.S., Frail D.A., Kulkarni S.R. (2003). *ApJ* **594**, 674.
- Bloom J.S., Prochaska J.X., Pooley D. et al. (2006). *ApJ* **638**, 354.
- Bloom J.S., Perley D.A., Li W. et al. (2009). *ApJ* **691**, 723.
- Boër M., et al. (1988). *A&A* **202**, 117.
- Bontekoe T.J.R., Winkler C., Stacy J.G., Jackson P.D. (1995). *Ap&SS* **231**, 285.
- Bouwhuis M. on behalf of the ANTARES collaboration (2010). In Proc. of 31th ICRC, Lodz, arXiv:1002.0701.
- Briggs M.S., Connaughton V., Meegan C.A. et al. (2009). AIP Conf. Proc. **1133**, p. 40.
- Bromm V., Loeb A. (2002). *ApJ* **575**, 111.
- Burrows, D.N., Romano, P., Falcone, A. et al. (2005). *Sci.* **309**, 1833.
- Burrows D.N. (2010). in *Deciphering the ancient Universe with GRBs*, Kyoto, Apr. 2010, AIP (in press)
- Butler N.R., Li W., Perley D. et al. (2006). *ApJ* **652**, 1390.
- Cenko S.B., Fox D.B., Moon D.-S. et al. (2006). *PASP* **118**, 1396.
- Cenko S.B., Keleman J., Harrison F.A., et al. (2009). *ApJ* **693**, 1484.
- Cenko S.B., Frail D.A., Harrison F.A. et al. (2010a). *ApJ* **711**, 641.
- Cenko S.B., Frail D.A., Harrison F.A. et al. (2010b). *ApJ* (subm.; arXiv:1004.2900).
- Chen H.-W., Prochaska J.X., Bloom J.S., et al. (2005). *ApJ* **634**, L25.
- Chevalier R.A., Li Z.-Y. (1999). *ApJ* **520**, L29.
- Chincarini G., Mao J., Margutti R. et al. (2010). *MN* (subm., arXiv:1004.0901)
- Chevalier R.A., Li Z.-Y. (2000). *ApJ* **536**, 195.
- Connaughton V. (2002). *ApJ* **567**, 1028.
- Costa E., Frontera F., Heise J. et al. (1997). *Nat.* **387**, 783.
- Covino S., D'Avanzo P., Klotz A. (2008). *MN* **388**, 347.
- Curran P.A., Starling R.L.C., O'Brien P.T. et al. (2008). *A&A* **487**, 533.
- Della Valle M., Chincarini G., Panagia N. et al. (2006). *Nat.* **444**, 1050.
- Denisenko D.V., Terekhov O.V. (2008). *Astron. Lett.* **34**, 298.
- De Pasquale M., Piro L., Perna R., et al. (2003). *ApJ* **592**, 1018.
- Dessauges-Zavadsky M., Chen H.-W., Prochaska J.X. et al. (2006). *ApJ* **648**, L89.
- Eichler D., Livio M., Piran T., Schramm D.N. (1989). *Nat.* **340**, 126.
- Falcone A.D., Burrows D.N., Lazzati D. et al. (2006). *ApJ* **641**, 1010.
- Frail, D.A., Kulkarni, S.R., Nicastro L. et al. (1997). *Nat.* **389**, 261.
- Frail, D.A., Waxman, E., Kulkarni, S.R. (2000). *ApJ* **537**, 191.

- Frail D.A., Kulkarni, S.R., Sari R., et al. (2001). *ApJ* **562**, L55.
- Frail, D.A., Kulkarni, S.R., Berger, E. et al. (2003a). *AJ* **125**, 2299.
- Frail, D.A., Yost S.A., Berger E. et al. (2003). *ApJ* **590**, 992.
- Frail, D.A., Soderberg, A.M., Kulkarni, S.R. et al (2005). *ApJ* **619**, 994.
- Frontera F., Greiner J., Antonelli L.A., et al. (1998). *A&A* **334**, L69.
- Fryer C.L. (1999). *ApJ* **522**, 413.
- Fryer C.L., Heger A. (2005). *ApJ* **623**, 302.
- Fynbo J.P.U., Jensen B.L., Gorosabel J. et al. (2001). *A&A* **369** 373.
- Fynbo J.P.U., Watson D., Thöne C.C. et al. (2006). *Nat.* **444**, 1047.
- Fynbo J.P.U., Jakobsson P., Prochaska J.X. et al. (2009). *ApJS* **185**, 526
- Galama T.J., Vreeswijk, P.M., van Paradijs, J. et al. (1998a). *Nat.* **395**, 670.
- Galama T.J., Wijers R.A.M.J., Bremer M. et al. (1998b). *ApJ* **500**, L97.
- Gal-Yam A., Ofek E.O., Filippenko A.V., et al. (2002). *PASP* **114**, 587.
- Gal-Yam A., Fox D.B., Price P.A. et al. (2006a). *Nat.* **444**, 1053.
- Gal-Yam A., Ofek E.O., Poznanski D. et al. (2006b). *ApJ* **639**, 331.
- Gehrels N., Sarazin C.L., O'Brien P.T. et al. (2005). *Nat.* **437**, 851.
- Gehrels N., Norris J.P., Barthelmy S.D., et al. (2006). *Nat.* **444**, 1044.
- Gehrels N., Ramirez-Ruiz E., Fox D.B. (2009). *ARAA* **47**, 567.
- Gendre B., Corsi A., Piro L. (2006). *A&A* **455**, 803
- Gendre B., Klotz A., Palazzi E. et al. (2010). *MN* (in press; arXiv:0909.1167)
- Genet F., Granot J. (2009). *MN* **339**, 1328.
- Ghirlanda G., Ghisellini G., Nava L. (2010). *A&A* **510**, L7.
- Ghisellini G., Lazzati D. (1999). *MN* **309**, L7.
- Ghirlanda G., Ghisellini G., Lazzati D. (2004). *ApJ* **616**, 331.
- Goad M.R., Page K.L., Godet O. et al. (2007). *A&A* **468**, 103.
- Godet O., Page K.L., Osborne J. et al. (2007). *A&A* **471**, 385.
- Gou L.J., Mészáros P., Abel T., Zhang B. (2004). *ApJ* **604**, 508.
- Granot, J., Ramirez-Ruiz, E., Loeb, A. (2005). *ApJ*, **618**, 413.
- Greiner J., Flohrer J., Wenzel W., Lehmann T. (1987). *ASS* **138**, 155.
- Greiner J., Wenzel W., Hudec R. et al.(1994). *Gamma-Ray Bursts*, eds. G.J. Fishman et al., AIP **307**, 408.
- Greiner J., Boër M., Kahabka P., Motch C., Voges W. (1995). NATO ASI **C450** *The Lives of the neutron stars*, eds. M.A. Alpar et al., Kluwer, p. 519.
- Greiner J., Bade N., Hurley K., Kippen R.M., Laros J., (1996). 3rd Huntsville workshop 1995, AIP **384**, p. 627.
- Greiner, J., Hartmann D., Voges W., et al. (2000). *A&A* **353**, 998.
- Greiner J., Klose S., Reinsch K. et al. (2003). *Nat.* **426**, 157.
- Greiner J., Bornemann W., Clemens C. et al. (2008). *PASP* **120**, 405.
- Greiner J., Clemens C., Krühler T. et al. (2009a). *A&A* **498**, 89.
- Greiner J., Krühler T., Fynbo J.P.U. et al. (2009b). *ApJ* **693**, 1610.
- Greiner J., Krühler T., Klose S. et al. (2010). *A&A* (subm).
- Grindlay J.E., Wright E.L., McCrosky R.E.: (1974). *ApJ* **192**, L113.
- Grupe D., Burrows D.N., Wu X.-F. et al. (2010). *ApJ* **711**, 1008.
- Grindlay J.E. (1999). *ApJ* **510**, 710.
- Guetta D. Stella L. (2009). *A&A* **498**, 329.
- Heger A., Langer N., Woosley S.E. (2000). *ApJ* **528**, 368.
- Heise J., in't Zand J., Kippen M., Woods P. (2001). in *GRBs in the afterglow Era*, Eds. E. Costa et al., ESO-Springer, 16.
- Harrison T.E., McNamara B.J., Pedersen H., et al.: (1995). *A&A* **297**, 465.
- Hjorth J., et al. (1999). *Sci.* **283**, 2073.



- Hjorth, J., et al. (2003). *Nat.* **423**, 847.
- Hoyle F. (1946). *MN* **106**, 343
- Hudec R., Borovicka, J., Wenzel, et al. (1987). *A&A* **175**, 71.
- Hurkett C.P., Vaughan S., Osborne J., et al. (2008). *ApJ* **679**, 587.
- Hurley K. (1999). *ApJS* **120**, 399.
- Hurley K., Costa E., Feroci M. et al. (1997). *ApJ* **485**, L1.
- Inoue A.K., Yamazaki R., Nakamura T. (2003). *ApJ* **601**, 644.
- Iwamoto et al. (1998). *Nat.* **395**, 672.
- Jelinek M., Prouza M., Kubanek P. et al. (2006). *A&A* **454**, L119.
- Kaneko Y., Ramirez-Ruiz E., Granot J., Woosley S., et al. (2007). *ApJ* 654, 385.
- Kann D.A., Klose S., Zeh A. (2006). *ApJ* **641**, 993.
- Kann D.A., Klose S., Zhang B., et al. (2010). *ApJ* (arXiv:0712.2186v2 from Sep. 2009).
- Kehoe R., Akerlof C.W., Balsano R., et al. (2002). *ApJ* 577, L159.
- Kippen R.M., et al., (1994). *Gamma-Ray Bursts*, eds. G.J. Fishman et al., AIP **307**, 418.
- Klose S., Henden A.A., Greiner J. et al. (2003). *ApJ* **592**, 1025.
- Klotz A., Gendre B., Stratta G., et al. (2006). *A&A* **451**, L39.
- Klotz, A., Boër, M., Atteia, J.L., Gendre, B. (2009). *AJ* **137**, 4100.
- Kobayashi S. (2000). *ApJ* **545**, 807.
- Kogut A., Spergel D.N., Barnes C. et al. (2003). *ApJS* **148**, 161.
- Kouveliotou, C., et al. (1993). *ApJ* **413**, L101.
- Krimm H., Vanderspek R.K., Ricker G.R.: (1994). *Gamma-Ray Bursts*, eds. G.J. Fishman et al., AIP **307**, 423.
- Krimm H.A., Granot J., Marshall F.E. et al. (2007). *ApJ* **665**, 554.
- Krühler T., Küpcü Yoldaş A., Greiner J. et al. (2008). *ApJ* **685**, 376.
- Krühler T., Greiner J., McBreen S. et al. (2009). *ApJ* **697**, 758.
- Kulkarni S.R., Rau A. (2006). *ApJ* **644**, L63.
- Kumar P., Panaitescu A. (2000). *ApJ* **541**, L51.
- Küpcü Yoldaş A., Greiner J., Perna R. (2006). *A&A* **457**, 115.
- Lamb D.Q., Reichart D.E. (2001). in *GRBs in the afterglow era*, eds. Costa et al. ESO-Springer, p. 226.
- Lamb D.Q., Donaghy T.Q., Graziani C. (2005). *ApJ* **620**, 355.
- Lazzati D., Ramirez-Ruiz E., Ghisellini G. (2001). *A&A* **379**, L39.
- Lazzati D., Rossi E., Covino S., Ghisellini G., Malesani D. (2002). *A&A* 396, L5.
- Ledoux C., Vreeswijk P.M., Smette A. et al. (2009). *A&A* **506**, 661.
- Levesque E., Berger E., Kewley L., Bagley M.M. (2010). *AJ* **139**, 694.
- Levinson A., Ofek E.O., Waxman E., Gal-Yam A. (2002). *ApJ* **576**, 923.
- Li P., Hurley K., Sommer M., et al. (1993). *BAAS* **25**, 846.
- Li W., Filippenko A.V., Chornock R., Jha S. (2003). *ApJ* **586**, L9.
- Lipkin, Y.M., Ofek, E.O., Gal-Yam, A. et al. (2004). *ApJ* **606**, 381.
- Lithwick Y., Sari R. (2001). *ApJ* **555**, 540.
- Loeb A., Barkana R. (2001). *ARAA* **39**, 19.
- Madau P., Della Valle M., Panagia N. (1998). *MN* **297**, L17
- Mao S., Mo H.J. (1998). *A&A* **339**, L1.
- McBreen S., Krühler T., Rau A. et al. (2010). *A&A* **516** (in press; arXiv:1003.3885)
- MacFadyen A.I., Woosley S.E. (1999). *ApJ* **524**, 262.
- Mazzali P.A., Deng J., Nomoto K. et al. (2006). *Nat.* **442**, 1018.
- Mészáros P., Rees M.J., Wijers R.A.M.J. (1998). *ApJ* **499**, 301.
- Mészáros P., Rees M. (1999). *MN* **306**, L39.

- Metzger M.R., Djorgovski S.G., Kulkarni S.R. et al. (1997). *Nat.* **387**, 878.
- Metzger B.D., Quatert E., Thompson T.A. (2008). *MN* **385**, 1455.
- Miralda-Escudé J. (2003). *Sci.* **300**, 1904.
- Molinari E., Vergani S.D., Malesani D. et al. (2007). *A&A* **469**, L13.
- Nakar E., Piran T. (2003). *New Astron.* **8**, 141.
- Nishihara E., Hashimoto O., Kinugasa K. (2003). GCN 2118.
- Nomoto K., Maeda K., Mazzali P.A. et al. (2004). in *Stellar Collapse*, eds C.L. Fryer, *ASSL* **302**, p. 277.
- Norris J.P., Bonnell J.T. (2006). *ApJ* **643**, 266.
- Norris J.P., Gehrels, N., Scargle, Jeffrey D. (2010). *ApJ* **717**, 411.
- Noterdaeme P., Ledoux C., Petitjean P., & Srinand R. (2008). *A&A* **481**, 327.
- Nousek J.A., Kouveliotou C., Grupe D., et al. (2006). *ApJ* **642**, 389.
- Oates S.R., Page M.J., Schady P. et al. (2009). *MN* **395**, 490.
- Oren Y., Nakar E., Piran T. (2005). *MN* **353**, L35.
- Paczynski B. (1998). *ApJ* **494**, L45.
- Panaiteanu A., Kumar, P. (2001). *ApJ* **554**, 667.
- Panaiteanu A., Kumar, P. (2002). *ApJ* **571**, 779.
- Panaiteanu A., Vestrand W.T. (2008). *MN* **387**, 497.
- Paragi Z., Taylor G.B., Kouveliotou C. et al. (2010). *Nat.* **463**, 516.
- Perley D.A., Bloom J.S., Butler N.R. et al. (2008). *ApJ* **672**, 449.
- Perley D.A., Cenko S.B., Bloom J.S., et al. (2009). *AJ* **138**, 1690.
- Perna R., Loeb A. (1998). *ApJ* **509**, L85.
- Perna, R., Raymond, J., Loeb, A. (2000). *ApJ* **533**, 658.
- Pihlström, Y.M., Taylor, G.B., Granot, J., Doeleman, S. (2007). *ApJ* **664**, 411.
- Piro L. (2001). in *GRBs in the Afterglow era*, eds. E. Costa, F. Frontera, J. Hjorth, Springer, Berlin, p. 97.
- Piro L., Scarsi L. (2004). in *The Restless High-Energy Universe*, May 2003, Amsterdam, Eds. E.P.J. van den Heuvel, R.A.M.J. Wijers, J.J.M. in 't Zand, *Nucl. Phys. B* (Proc. Suppl.) **132**, p. 3.
- Pizzichini G., et al. (1986). *ApJ* **301**, 641.
- Porciani C., Viel M., Lilly S.J. (2007). *ApJ* **659**, 218.
- Price P.A., Fox D.W., Kulkarni S.R., et al. (2003). *Nat.* **423**, 844.
- Podsiadlowski P., Mazzali P.A., Nomoto K. et al. (2004). *ApJ* **607**, L51.
- Prochaska J.X., Chen H.-W., Bloom J.S. (2006). *ApJ* **648**, 95.
- Prochter G.E., et al. (2006). *ApJ* **648**, L93.
- Quimby R.M., Rykoff E.S., Yost S.A. et al. (2006). *ApJ* **640**, 402.
- Racusin J.L., Karpov S.V., Sokolowski M., et al. (2008). *Nat.* **455**, 183.
- Racusin J.L., Liang E.W., Burrows D.N. et al. (2009). *ApJ* **698**, 43.
- Rau A., Greiner J., Schwarz R., (2006). *A&A* **449**, 79.
- Rau A., Savaglio S., Krühler T. et al. (2010). *ApJ* (subm.; arXiv:1004.3261).
- Resmi, L., Ishwara-Chandra, C.H., Castro-Tirado A.J. et al (2005). *A&A* **440**, 477.
- Rhoads J.E., (1997). *ApJ* **487**, L1.
- Rhoads J.E., (1997). *ApJ* **525**, 737.
- Richardson D. (2009). *AJ* **137**, 347.
- Ricker G.R., Atteia J.-L., Crew G.B. et al. (2002). in *GRB and Afterglow Astronomy 2001* ed. G.R. Ricker & R.K. Vanderspek (New York) AIP **662**, p. 3.
- Rol, E., et al. (2000). *ApJ* **544**, 707.
- Romano P., Campana S., Mignani R.P., et al. (2008). *VizieR Online Data Catalog* 348:81221.

- Rossi A., Schulze S., Klose S. et al. (2010). *A&A* (subm.; arXiv:1007.0383)
- Rykoff E., Smith D.A., Price P.A. et al. (2004). *ApJ* **601**, 1013.
- Rykoff E., Aharonian F., Akerlof C.W., et al. (2005). *ApJ* **631**, 1032.
- Rykoff E., Aharonian F., Akerlof C.W., et al. (2009). *ApJ* **702**, 489.
- Sakamoto T., Hullinger D., Sato G. et al. (2008). *ApJ* **679**, 570.
- Salvaterra, R., Della Valle, M., Campana, S. et al. (2009). *Nat.* **461**, 1258.
- Sari R., Piran T., Narayan R. (1998). *ApJ* **497**, L17.
- Sari R. (1999). *ApJ* **524**, L43.
- Sari R., Piran T. (1999). *ApJ* **517**, L109.
- Savaglio, S., Glazebrook, K., Le Borgne, D. (2009). *ApJ* **691**, 182.
- Schaefer B.E., Bradt, H., Barat, C. et al. (1984). *ApJ* **286**, L1.
- Schady P., Mason K.O., Page M.J. et al. (2007). *MN* **377**, 273.
- Schady P., Page M.J., Oates S.R. et al. (2010). *MN* **401**, 2773.
- Schmidt M. (2000). *ApJ* **552**, 36.
- Smartt S.J., Vreeswijk P.M., Ramirez-Ruiz E. et al. (2002). *ApJ* **572**, L147.
- Soderberg A.M., Chakraborti S., Pignata G. et al. (2010). *Nat.* **463**, 513.
- Spruit H. (2002). *A&A* **381**, 923.
- Stanek K., et al. (2003). *ApJ* **591**, L17.
- Steele I.A., Mundell C.G., Smith R.J., Kobayashi S., Guidorzi C. (2010). *Nat.* **462**, 767.
- Stratta G., Fiore F., Antonelli L.A. et al. (2004). *ApJ* **608**, 846.
- Sudilovsky V., Savaglio S., Vreeswijk P.M. et al. (2007). *ApJ* **669**, 741.
- Tagliaferri, G., Goad, M., Chincarini, G. et al. (2005). *Nat.* **436**, 985.
- Tanvir N.R., Fox D.B., Levan A.J. et al. (2009). *Nat.* **461**, 1254.
- Taylor, G.B., Frail, D.A., Berger, E., Kulkarni, S.R. (2004). *ApJ* **609**, L1.
- Tejos N., Lopez S., Prochaska J.X. et al. (2009). *ApJ* **706**, 1309.
- Troja E., King A.R., O'Brien P.T. et al. (2008). *MN* **385**, L10.
- Vanden Berk D.E., Lee B.C., Wilhite B.C. et al. (2002). *ApJ* **576**, 673
- Van der Horst, A.J., Kamble, A., Resmi, L. et al. (2008). *A&A* **480**, 35.
- Vanderspek R., Krimm H.A., Ricker G.R.: (1994). *Gamma-Ray Bursts*, eds. G.J. Fishman et al., AIP **307**, 438.
- Vanderspek R.K., Krimm H.A., Ricker G.R.: (1995). *Ap&SS* **231**, 259.
- Van Paradijs, J. Groot, P.J., Galama, T. et al. (1997). *Nat.* **386**, 686.
- Vergani S.D., Petitjean P., Ledoux C. et al. (2009). *A&A* **503**, 771.
- Vestrand W.T., Borozdin K., Caspersen D.J. (2004). *AN* **325**, 549.
- Vestrand W.T., Wozniak, P.R., Wren, J.A. et al. (2005). *Nat.* **435**, 178.
- Vestrand W.T., Wren, J.A., Wozniak, P.R. et al. (2006). *Nat.* **442**, 172.
- Villasenor J., Ricker G., Vanderspek R. et al. (2004). in *Proc. 35th COSPAR Sci. Assembly*, July 2004, Paris, p. 1225.
- Villasenor J., Lamb D.Q., Ricker G. et al (2005). *Nat.* **437**, 855.
- Vink J.S., de Koter A. (2005). *A&A* **442**, 587.
- Virgili F.J., Zhang B., O'Brien P.T., Troja E. (2010). *ApJ* (subm.; arXiv:0909.1850)
- Vreeswijk P.M., Ellison S.L., Ledoux C. et al. (2004). *A&A* **419**, 927.
- Vreeswijk P.M., Ledoux C., Smette A. et al. (2007). *A&A* **468**, 83.
- Waxman E. (1997). *ApJ* **489**, L33.
- West J.P., McLin K., Brennan T. et al. (2008). GCN 8617.
- Wijers, R.A.M.J., Galama T.J. (1999). *ApJ* **523**, 177.
- Wijers, R.A.M.J., et al. (1999). *ApJ* **523**, L33.
- Woosley S.E., Heger A. Weaver T.A. (2002). *Rev. Mod. Phys.* **74**, 1015.
- Woosley S.E., Bloom J.S. (2006). *ARAA* **44**, 507.

- Yoon S.-C., Langer N. (2005). *A&A* **443**, 643.  
Yost S.A., Frail D.A., Harrison F.A. et al. (2002). *ApJ* **577**, 155.  
Yost S.A., Alatalo K., Rykoff E.S., et al. (2006). *ApJ* **636**, 959.  
Yuan F., Rujopakarn W. (2008). GCN 8536.  
Zhang B., Fan Y.Z., Dyks J. et al. (2006). *ApJ* **642**, 354.  
Zhang, B., Zhang, B.-B., Virgili, F.J. et al. (2009). *ApJ* **703**, 1696.

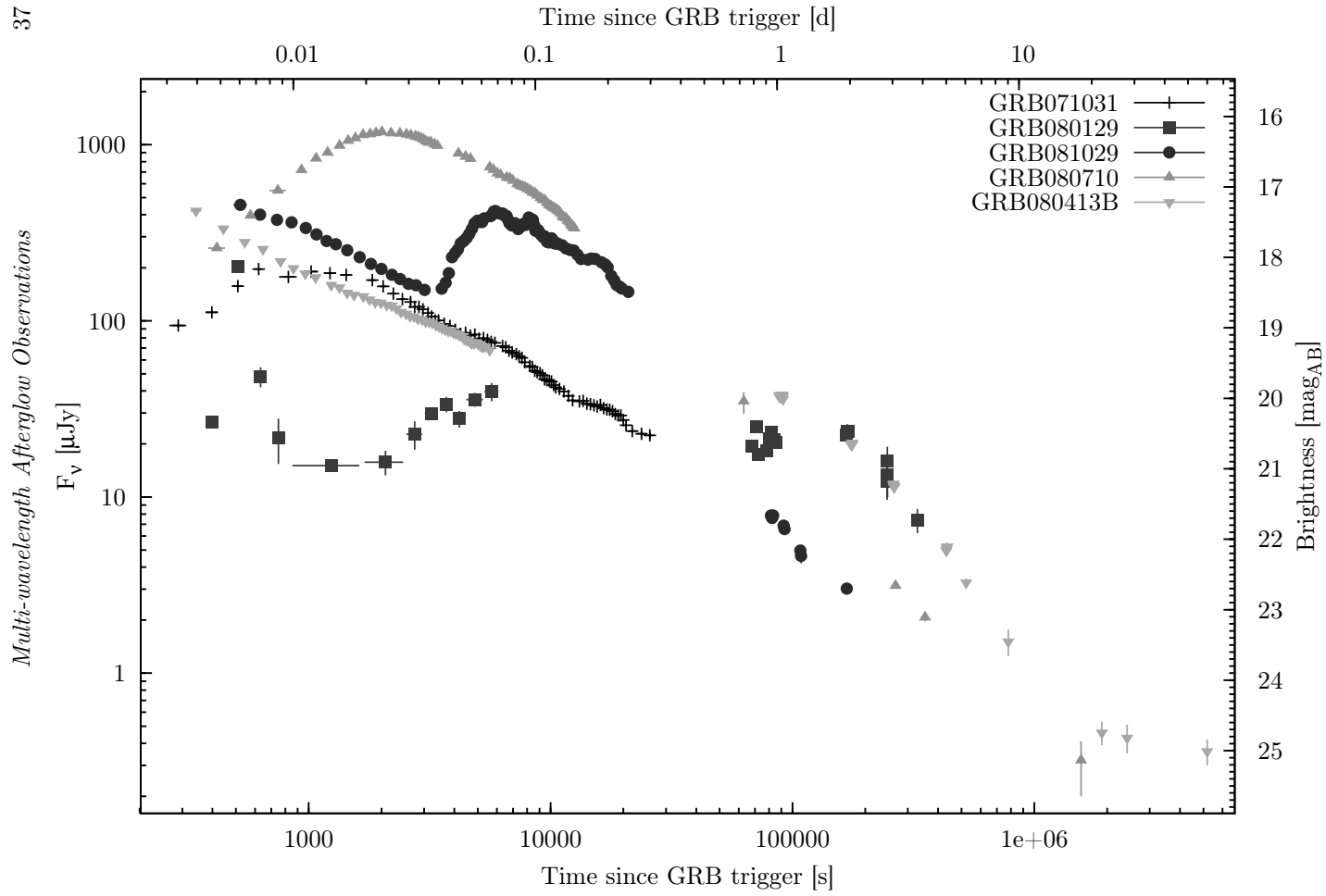


Fig. 6.4. Representative examples of optical light curves of long-duration GRBs as measured with GROND. The light curve diversity is similar to that in X-rays.

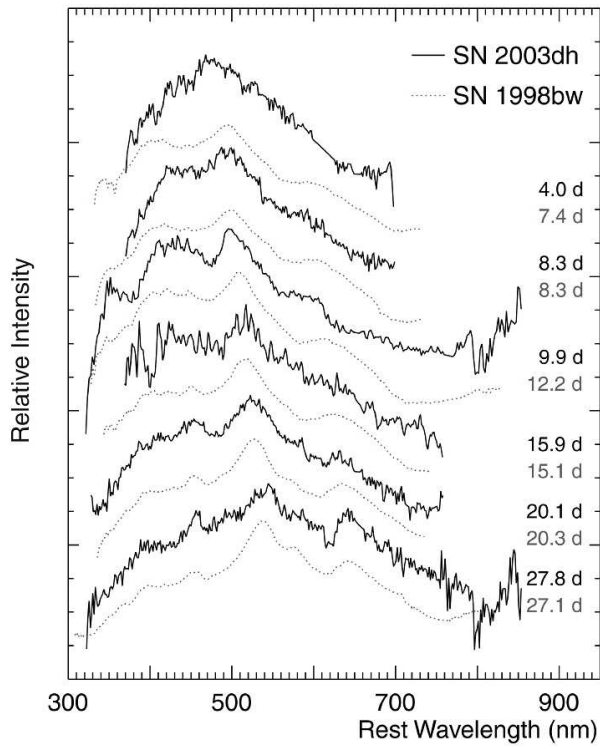


Fig. 6.5. Evolution of the optical spectrum of the afterglow of GRB 030329 showing features of a SN Ic, as compared to the spectra of SN 1998bw (dotted lines). The time after the SN explosion is given on the right side. From Hjorth et al. (2003)

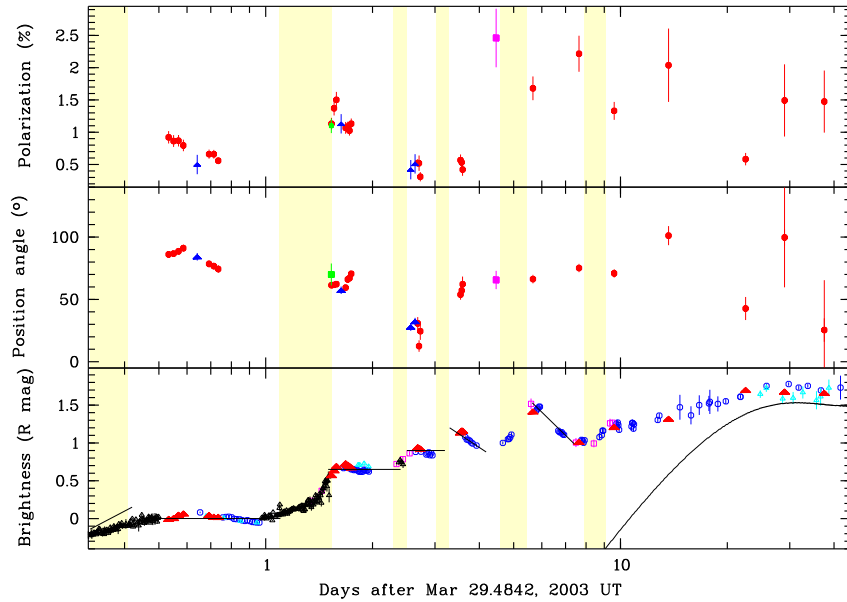


Fig. 6.6. Evolution of the polarization of the afterglow of GRB 030329 during the first 38 days. The top and middle panels show the polarization degree in percent and the position angle in degrees. The bottom panel shows the residual  $R$  band light curve after subtraction of a power-law  $t^{-1.64}$  describing the undisturbed decay during the time interval 0.5 – 1.2 days after the GRB, thus leading to a horizontal curve. Gray bars mark re-brightening transitions. Contributions from an underlying supernova (solid curved line) do not become significant until  $\sim 10$  days after the GRB. From Greiner et al. (2003)

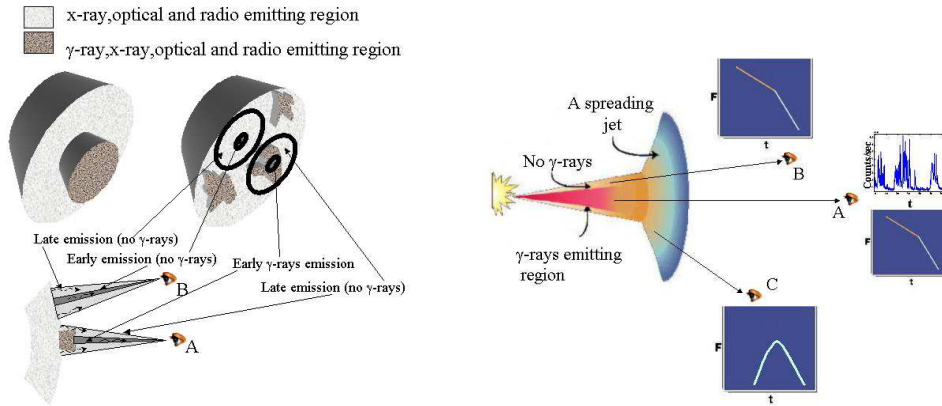


Fig. 6.7. **Left:** Schematics of an on-axis orphan afterglow: prompt gamma-rays are emitted only by some regions which can have either a regular (upper left; cross-section in the lower picture) or irregular structure (upper right). The ellipses describe the area seen by an observer at a given time. Observer A detects the early emission from a small region within the gamma-ray emitting region, and later an afterglow from a much larger region (regular GRB and afterglow). Observer B does not detect any gamma-rays, but detects a regular (on-axis orphan) afterglow. **Right:** An off-axis orphan afterglow is seen by observers which are not within the initial relativistic jet. This emission is seen only after the jet break. Observer A detects both, the GRB and the afterglow; observer B detects the same afterglow but no gamma-rays, and observer C detects an off-axis orphan afterglow. From Nakar & Piran (2003)

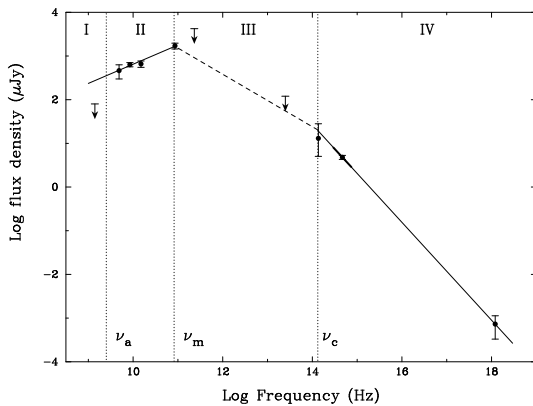


Fig. 6.8. X-ray-to-radio spectral energy distribution of GRB 970508 at 12.1 days after the burst. Indicated are the inferred values of the break frequencies  $\nu_a$ ,  $\nu_m$  and  $\nu_c$ . From Galama et al. (1998b).



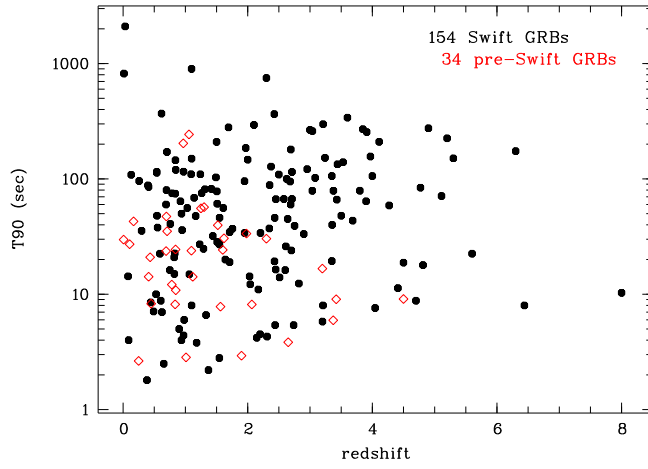


Fig. 6.9. Rest-frame duration of long GRBs versus redshift. The predicted trend of larger  $T_{90}$  with redshift  $z$ , is not obvious. Filled symbols denote *Swift* GRBs, while open triangles denote pre-*Swift* era bursts (which have a different bias in the  $T_{90}$  determination).

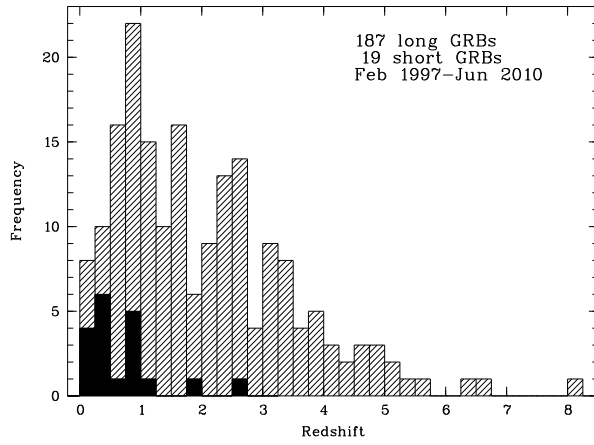


Fig. 6.10. Observed redshift distribution of long- (grey) and short-duration (black) GRBs as of June 2010.